POLITECNICO DI TORINO

Corso di Laurea Magistrale in Ingegneria Aerospaziale

Tesi di Laurea Magistrale

Study of the drone propulsion system for high altitude operations

Relatore:
Prof. Paolo Maggiore
Correlatore:
Prof. Domenic D'Ambrosio

Candidato:
Antonino Alesci

Anno Accademico 2018/2019

Ringraziamenti

Grazie di cuore alla mia famiglia, Mamma, Papà, Gianmarco e soprattutto a te Floriana. Grazie

Abstract

The following thesis, carried out in collaboration with the company Pro S3 s.r.l., consists in the study of the propulsion system of a quadricopter drone, with the aim of developing four propellers for vertical take-off and a propeller for horizontal flight. The Skywalker X8 drone must operate at an altitude of 4000 m.

The theories used are: Simple Impulsive Theory, Extended Impulsive Theory, Vortex Theory, Blade Element Theory, and Linearized theory of the actuator disk.

Firstly, the drone characteristics and the operating environment, characterized by a density of $0.86\ kg/m^3$, are exposed; the density is of central importance because, by calculating the Reynolds number, it contributes to the determination of the flow.

Later, the Simple Impulsive Theory and the Extended Impulsive Theory are discussed and applied by considering a determined number of scenarios characterized by masses and variable diameters. The aim concerns the determination of the induced power and the induced speed for each scenario.

The application of the Vortex Theory allows to calculate the vorticity distribution under optimal conditions by determining the load parameter of Glauert (G) using an iterative method. Moreover, this theory is applied both to a disk with an infinite number of blades and to a disk with finite number of blades, considering, at the same time, the losses at the tip by using the Prandtl factor.

The Linearized theory of the actuator disk identifies the motion field induced by the propeller.

Finally, the results obtained from the application of these theories, the profiles used, with the corresponding performance calculated with XFOIL, and the motion field results are reported.

Index

Figure Index

Table Index

1 – Introduction

The following thesis aims to develop four propellers for vertical take-off and one for the straight horizontal flight of the Skywalker X8 drone.

The drone in question has to operate at high altitude, about 4000 m, and it has to carry out activities such as shooting or photographs.

The following thesis work was carried out in collaboration with the company Pro S3 s.r.l.

1.2 - The drone Skywalker X8

The following drone can be found in two configurations, one with the presence of four arms used for placing the four propellers and one without the following arms, but with a single propeller. In the latter case, the take-off is performed in a special ramp.

Figure 1 - First configuration

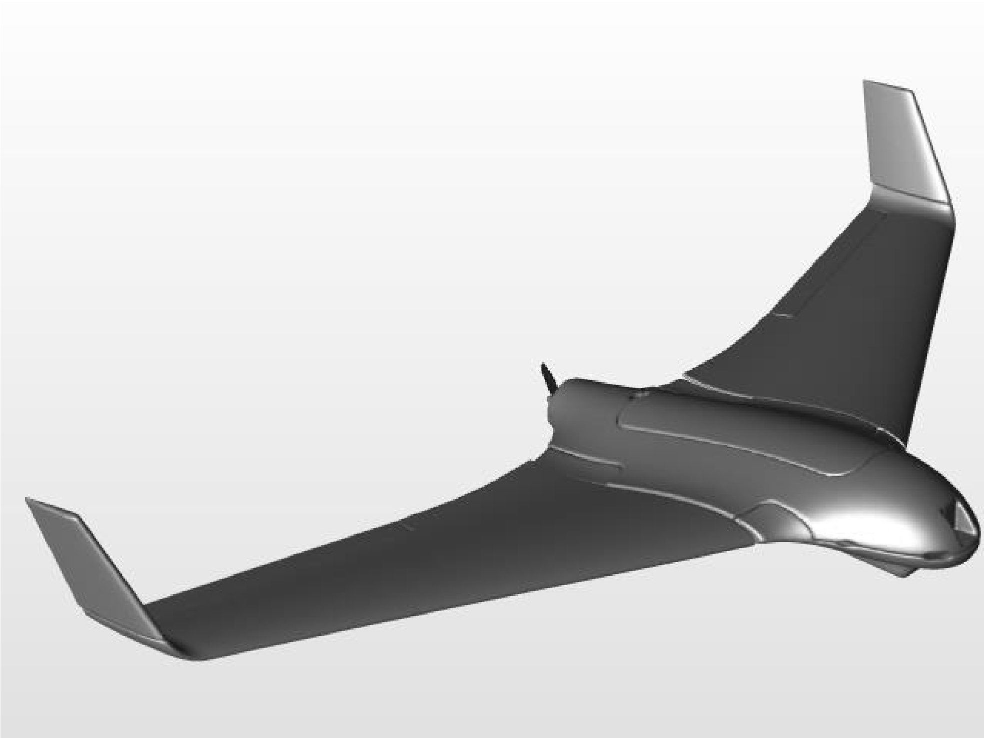

Figure 2 - Second configuration

The configuration discussed in the thesis is the first one (Figure 1). The drone consists of:

- Wing span: $2.122\ [m]$
- Length: 0.82 $[m]$
- Mass: $4\ [kg]$
- Cruise speed: 19 $[m/s]$

1.2 – Environment

The operating environment is relative to 4000 m, therefore the operations take place inside the troposphere, which is in contact with the earth's surface and extends up to 16-20 km to the equator and up to 8 km to the poles.

The troposphere contains the ¾ of the entire gaseous mass and in it mainly occur the atmospheric phenomena which consists of (Saha, 2008):

- Nitrogen: 78.09%
- Oxygen: 20.95%
- Argon: 0.93%
- The last percentage is about the other gas

Regarding physical quantities:

Table 1 - Atmosphere at 4000 m

Temperature	$262.15\ [K]$
Pressure in ISA condition	$6.5 \cdot 10^4\ [Pa]$
Density	$0.8631\ [kg/m^3]$
Dynamic viscosity	$1.665 \cdot 10^{-5}$
Cinematic viscosity	$1.929 \cdot 10^{-5}$
Speed of sound	$324.72\ [m/s]$
Gravity acceleration	$9.81\ [m/s^2]$

Figure 3 - layers of the atmosphere

2 - Momentum theory

The momentum theory was made to develop propellers used in the nautical field. The following theory was determined by W.J.M Rankine (1865) and R.E. Froude (1885); then, it was extended by A. Betz in 1920, also considering slipstream rotation.

The actuator disk supports the thrust explained in the following paragraph, and the direction of the air is opposite to the thrust; for this reason, it leads back to Newton's third law (reaction action law).

The wake stream has specific kinetic energy, from the latter, it is possible to determine the induced power, linked to the induced resistance of a fixed-wing.

This theory does not allow to obtain essential data relating to the flow; moreover, it needs the application of conservation laws.

2.1 - Analytical treatment (Simple Impulsive Theory)

Before explaining the momentum theory, it is necessary an introduction relating to the actuator disk, exploited precisely within the theory just mentioned to simplify it.

The actuator disk is a simplified model of the rotor, consisting of a circular section of infinitesimal thickness.

- The actuator disk is rotated through a torque, which determines a certain angular momentum on the fluid.
- The thrust on the rotor has a uniform distribution, and an instantaneous pressure variation (ΔP) occurs through the circular surface selected by an infinitesimal thickness. The uniform thrust can be realized because the rotor has an infinite number of blades.
- "*The slipstream of the rotor is a clearly defined mass of moving air outside which the air is practically undisturbed*" (A. R. S. Bramwell, 2001).
- The flow is ideal, steady and irrotational.

Through the preliminary analysis, that it is carried out later, all that is done to know the flow velocity and the power, according to the thrust determined in the preliminary phase. These physical quantities are obtained by considering the influence of the actuator disk on the flow, and through the momentum theory, this problem is solved by applying the conservation laws.

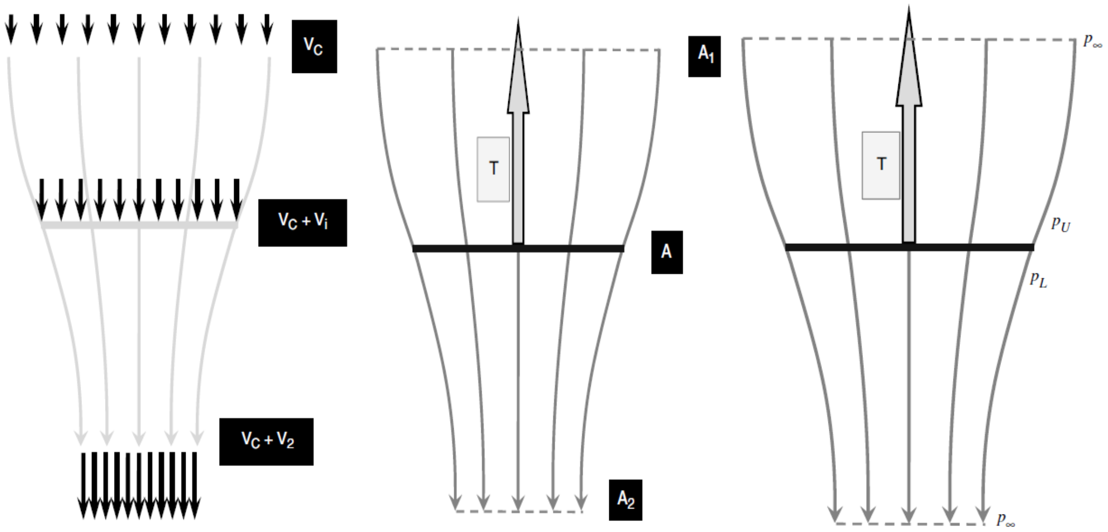

Figure 4 - Variation throw the actuator disk in vertical flight

- V_c: represents the ascent speed.
- V_i: represents the increase in speed that the disk provides to the flow.
- T: thrust generated by the disk and opposite to the fluid direction.
- V_2: speed increase downstream of the flow tube.
- P_U, P_L: represent the pressure before and after the actuator disk, and the difference between them gives the pressure increment (ΔP)

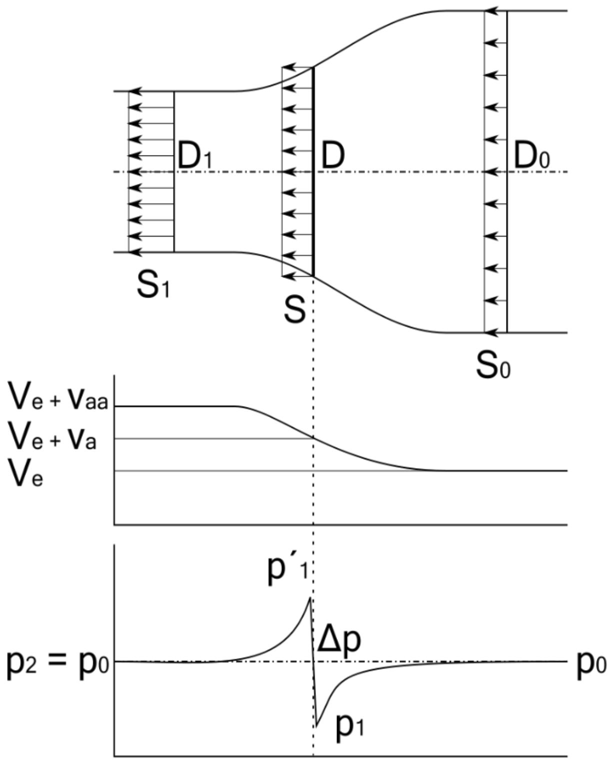

Figure 5 - Graphical point of view

This theory considered an actuator disk constituted by an area: $A = \pi \cdot R^2$. The mass flow rate that crosses the surface of the disk is $\dot{m} = \rho A V$, which is constant.

The thrust generated is expressed as:

$$T = \int_{A_d} \Delta P \cdot dA = \int_0^{R_d} \Delta p \cdot 2\pi r \cdot dr \tag{2.1}$$

If the pressure variation is constant, it is possible to take it out of the integral obtaining:

$$T = \Delta p \cdot A_d \tag{2.2}$$

Applying the Bernoulli equation to the various stations (Figure 3):

- Station 0 – 2:

$$P_0 = P_2 + \frac{1}{2}\rho v^2$$

- Station 3 – 1

$$P_3 = \frac{1}{2}\rho v^2 = P_0 + \frac{1}{2}\rho w^2$$

From the combination of the following equations, it is possible to obtain the thrust per unit area:

$$\frac{T}{A} = P_3 - P_2 = \frac{1}{2}\rho w^2 \tag{2.3}$$

Considering the mass flow through the disc:

$$T \cdot v = \frac{1}{2}\dot{m} w^2 \tag{2.4}$$

- Station 0 – 1:

Now in the equation (2.5), the whole tube, from the input surface to the output surface, is considered:

$$T = \rho (V_C + w)^2 A_\infty - \rho V_C^2 A_0 \tag{2.5}$$

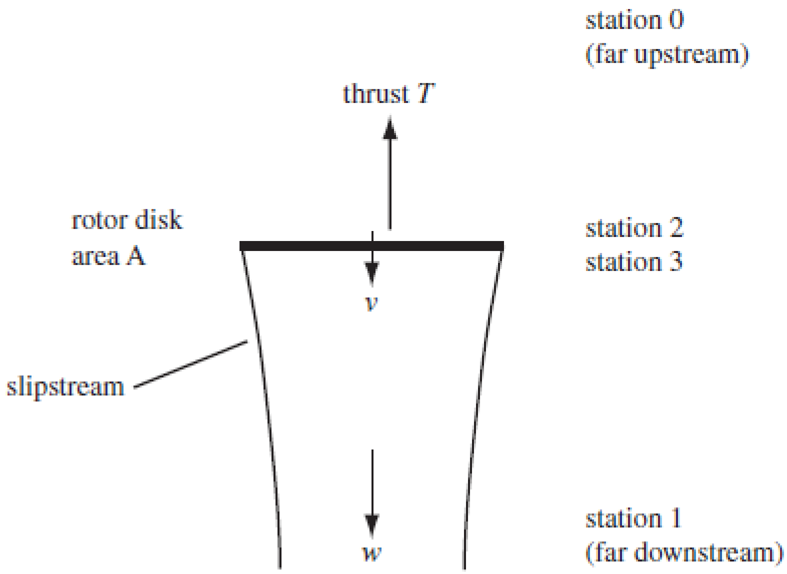

Figure 6 - Flow tube with stations

In the flow tube, there is an increase in speed, this increment determines an instantaneous reduction in pressure, as shown in Figure 5, and a reduction in the section of the flow tube to satisfy the conservation mass low. In the case of incompressible fluid, the mass flow rate remains constant, also considering the stationary flow condition, then the mass conservation law can be expressed in terms of volume obtaining Leonardo's law:

$$V \cdot A = cost. \tag{2.6}$$

Equation (2.6) is constant for each section of the flow tube.

$$V_C \cdot A_0 = (V_c + w) \cdot A_\infty = (V_c + v_i) \cdot A_d \tag{2.7}$$

From equation (2.7) it is possible to derive the equation of the areas (A_∞ and A_0) and replace them in equation (2.5) obtaining:

$$T = \frac{\rho \pi D_d^2}{4} \cdot (V_c + v_i) \cdot w \tag{2.8}$$

Considering the equation reported (2.9):

$$p + \frac{1}{2}\rho V^2 + \rho g z = cost. \tag{2.9}$$

The (2.9) represents the Bernoulli equation, and in the case of negligible variations of the height, the third term is negligible, and it is possible to explain the pressure difference as:

$$\Delta p = \rho w \left(V_C + \frac{1}{2} w\right) \tag{2.10}$$

Replacing equation (2.10) in (2.2) it is possible to obtain the Froude's Theorem, which affirm that the velocity induced at the infinite downstream (w) is precisely twice the speed estimated at the actuator disk (v_i).

The theorem just explained allows to rewrite the equation (2.8) and (2.10) reporting only the speed evaluated at the disk:

$$T = \frac{\rho \pi D_d^2}{2}(V_C + v_i)v_i \tag{2.11}$$

$$\Delta p = 2\rho v_i (V_C + v_i) \tag{2.12}$$

In the previous equations V_C, is the climb speed.

If the flight is not vertical, but there is a hover condition, the climb speed (V_C) is zero, and the lift generated by the actuator disk is equal in module to the weight, but the opposite direction.

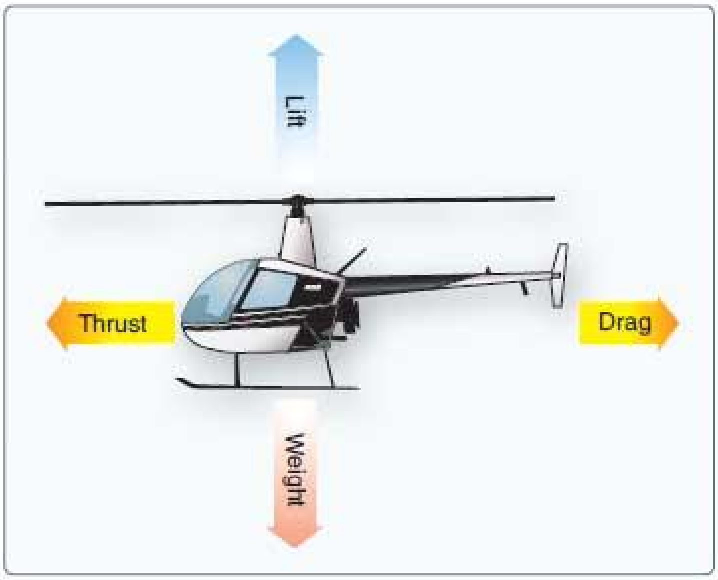

Figure 7 - Helicopter hovering flight

$$T = \frac{\rho \pi D_d^2}{2}(V_C + v_i) \cdot v_i \tag{2.13}$$

$$\Delta p = 2\rho v_i (V_C + v_i) \tag{2.14}$$

The Simple Impulsive Theory is applied to make an example of this model. It is considered a certain number of masses and diameters, and from the combination, a certain number of scenarios are performed. It should be noted that all the calculations are carried out considering an altitude of 4000 m, therefore with density present at the considered level.

Table 2 - Masses

Masses $[kg]$									
0.125	0.25	0.375	0.5	0.625	0.75	0.875	1	1.125	1.25
1.375	1.5	1.625	1.75	1.875	2	2.125	2.25	2.375	2.5

Table 3 - Diameters

Diameters $[m]$									
0.10	0.11	0.11	0.12	0.13	0.13	0.14	0.15	0.16	0.16
0.17	0.18	0.18	0.19	0.20	0.20	0.21	0.22	0.22	0.23
0.24	0.24	0.25	0.26	0.27	0.27	0.28	0.29	0.29	0.30

Table 4 - Necessary thrust

Thrust $[N]$									
1.23	2.45	3.68	4.91	6.13	7.36	8.58	9.81	11.04	12.26
13.49	14.72	15.94	17.17	18.39	19.62	20.85	22.07	23.30	24.53

The speeds belonging to each scenario are obtained with equation (2.15), and the induced power (2.16)

$$v_i = \sqrt{\frac{2 \cdot T}{\pi \rho D_d^2}} \tag{2.15}$$

$$P_i = T \cdot v_i \tag{2.16}$$

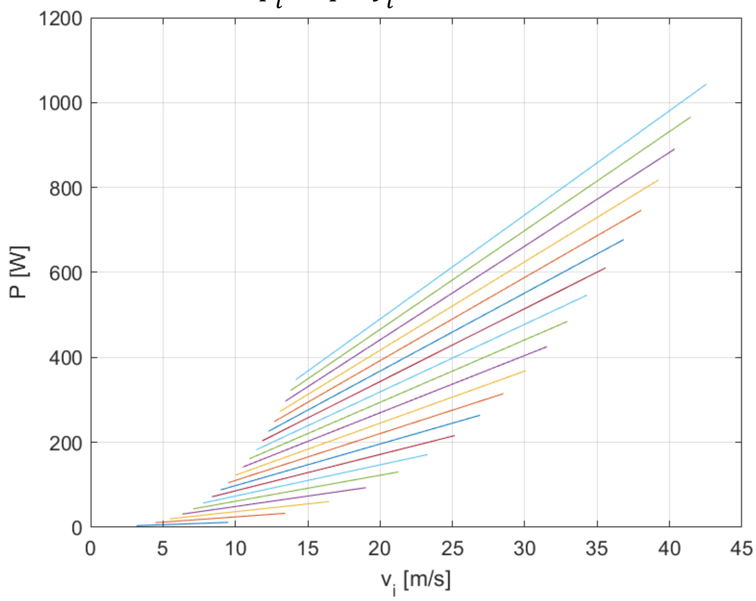

Figure 8 - Induced power

In Figure 8, the curves are parameterized with the mass, in particular, the value of the powers increases as the mass increases

2.2 - Analytical treatment (Extended Impulsive Theory)

The Simple Impulsive Theory considers stationary, incompressible, and irrotational flux; in the extended theory, instead, the condition of irrotational flux is no longer considered, and the vorticity downstream of the rotor is also taken into account. The conservation laws are always used, with the addition of the conservation of the angular momentum due to the rotation of the wake downstream of the disc.

The laws in use are the following:

- Conservation of the mass

$$\rho \int \boldsymbol{q} \cdot \boldsymbol{n}\, dS = 0 \tag{2.16}$$

- Conservation of momentum

$$\rho \int \boldsymbol{q}\boldsymbol{q} \cdot \boldsymbol{n}\, dS + \int p\, \boldsymbol{n}\, dS = F_{body} \tag{2.17}$$

- Conservation of angular momentum

$$\rho \int \boldsymbol{r} \times \boldsymbol{q}\boldsymbol{q} \cdot \boldsymbol{n}\, dS + \int p\boldsymbol{r} \times \boldsymbol{n}\, dS = M_{body} \tag{2.18}$$

- Energy conservation

$$\int \left(p + \frac{1}{2}\rho q^2\right) \boldsymbol{q} \cdot \boldsymbol{n}\, dS = \frac{dE}{dt} \tag{2.19}$$

dS represents the reference surface, and it encloses the fluid, n represents the normal to the surface. F_{body} and M_{body} represent the force and the moment acting on the rotor, while the ratio dE/dt represents the energy added to the flow by the rotor.

In this theory, a function of the radius must be obtained in such a way as to be able to minimize the power induced by a given thrust. It is possible to introduce the Lagrange multipliers to satisfy this request, which are chosen arbitrarily to find the minimum of the induced power.

With the extended impulsive theory, it is possible to identify the tangential and axial velocity knowing the thrust.

The thrust, power, and torque are calculated respectively:

$$T = \int_{A_d} \Delta p \cdot dA = \int_{S_1} \rho w^2\, dS_1 + \int_{S_1} (p_1 - p_0) dS_1 \tag{2.20}$$

$$P_i = \int_{A_d} \Delta P \cdot v \, dA + \int_{A_d} \frac{1}{2} \rho u^2 v \, dA \tag{2.21}$$

$$Q = \int_{A_d} \rho \cdot v \cdot u \cdot r \cdot dA = \int_{S_1} \rho \cdot w \cdot u_1 \cdot r_1 \, dS_1 \tag{2.22}$$

In the relations shown, the velocities u and v represent the tangential and axial velocity, respectively. Equation (2.21) consists of two terms; the first determines the acceleration of the fluid in the axial direction; the second term is not a power because the rotary motion does not determine thrust.

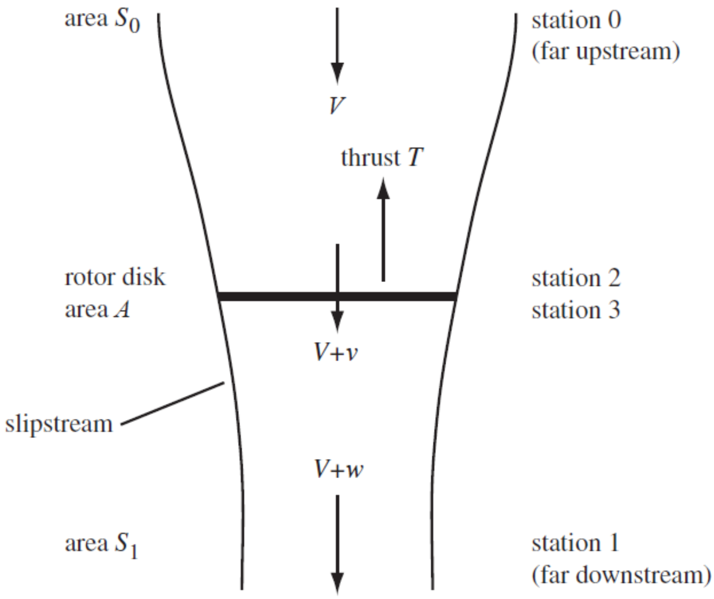

Figure 9 - Extended theory

The induced power reported in equation (2.21) is equal to the power calculated at the tree:

$$P = \Omega \cdot Q \tag{2.23}$$

By replacing in (2.23) equation (2.21) and (2.22), it is possible to get:

$$\int_{A_d} \Delta p \cdot v \, dA + \int_{A_d} \frac{1}{2} \rho u^2 v \, dA = \int_{A_d} \Omega \cdot \rho \cdot u \cdot v \cdot r \, dA \tag{2.24}$$

By manipulating this equation, the pressure difference is obtained:

$$\int_{A_d} \Delta p \cdot v \, dA = \int_{A_d} \rho v \left(\Omega r - \frac{1}{2} u \right) u \cdot dA$$

$$\Delta p \cdot v \, dA = \rho v \left(\Omega r - \frac{1}{2} u \right) u \cdot dA$$

$$\Delta p = \rho \left(\Omega r - \frac{1}{2} u \right) u \tag{2.25}$$

It is possible to replace the equation (2.25) in the (2.12) obtained in the previous paragraph.

$$2\rho v^2 = \rho\left(\Omega r - \frac{1}{2}u\right)u \tag{2.26}$$

$$2v^2 = \left(\Omega r - \frac{1}{2}u\right)u \tag{2.27}$$

Following the process reported in (Johnson W. , 2013), the optimal value of the tangential and axial velocity is determined by an iterative way to evaluate v_0 knowing the thrust T. The term v_0 has the same dimensions of the speed and is a free parameter which is determined, as just said, by the imposition of the thrust.

$$T = 2\rho v_0^2 \int \frac{(\Omega r)^4}{[(\Omega r)^2 + v_0]} dA \tag{2.28}$$

$$T = 2\rho A v_0^2 \left[1 + \frac{2v_0^2}{(\Omega R)^2} \cdot \ln\left(\frac{v_0}{\Omega R}\right) + \frac{v_0^2}{(\Omega R)^2}\right] \tag{2.29}$$

With equation (2.29) it is possible to determine the value of v_0 iteratively, after having determined it is possible to obtain:

$$u = \Omega r \cdot \frac{2v_0^2}{(\Omega r)^2 + v_0^2} \tag{2.30}$$

$$v = v_0 \cdot \frac{(\Omega r)^2}{(\Omega r)^2 + v_0^2} \tag{2.31}$$

Considering the scenarios described above and replacing v_0 in the equations (2.30) and (2.31), the tangential and axial speed distribution is determined.

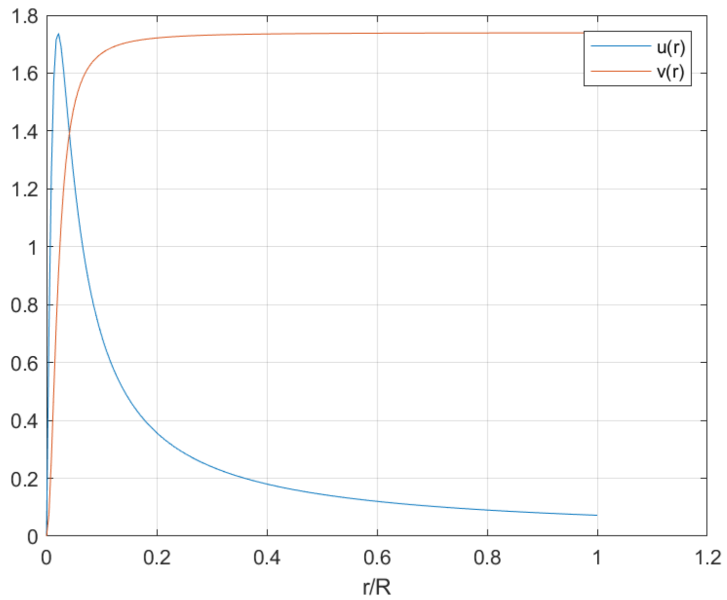

Figure 10 - Tangential and axial speed distribution

In the following treatment, the power is calculated considering the rotation of the wake, the following parameter is compared with the power induced by Simple Impulsive Theory to verify the increase.

$$P_u = \int v(r) \cdot dT \tag{2.32}$$

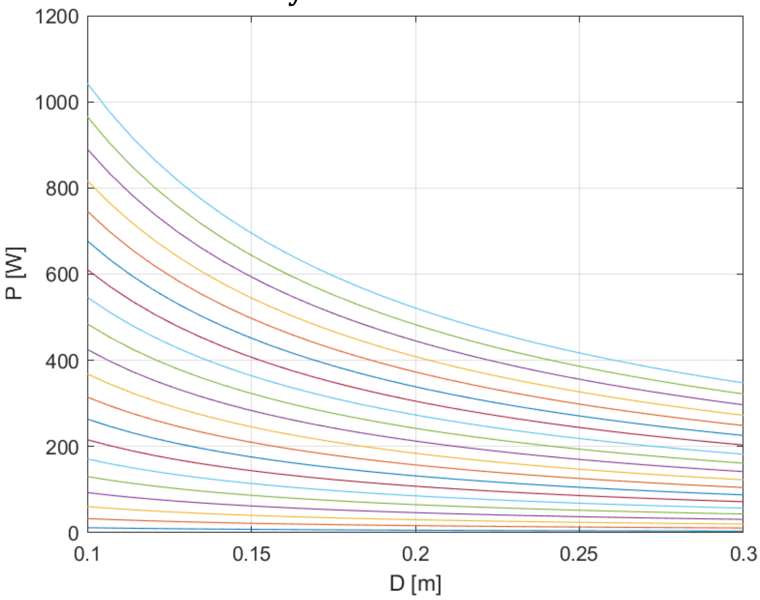

Figure 11 - TIS

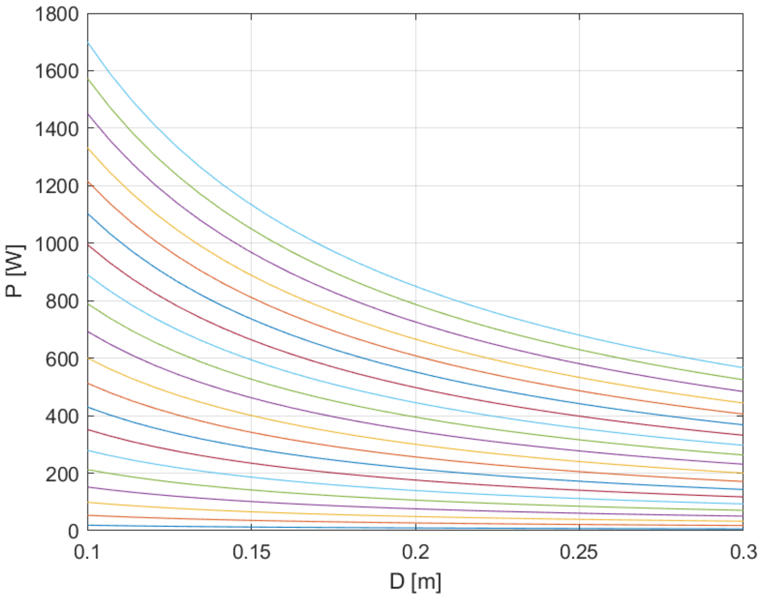

Figure 12 - TIE

In the following chapter, the application of the simple and extended impulsive theory has been reported to evaluate the effect of the rotation of the wake.

3 - Blade Element Theory

The first development of this theory, especially around 1920, followed two separate concepts: one was the blade element theory, the second was the momentum theory.

The first approaches of considerable importance date back to the studies of William Froude (1878) and Stefan Drzewiecki (1892-1920), who approached the study considering the independent airfoils profiles between them, in particular, his studies were uncertain due to the aerodynamic characteristics adopted for the profiles; to deal with this problem, an empirical approach was used, that was calculating the necessary characteristics directly on a series of propeller.

Therefore, using the characteristics of 2D profiles in the following analysis, give erroneous results, therefore Drzewiecki, used the characteristics related to the 3D wing to obtain acceptable results, even if there is a certain margin of error.

G. de Bothezat (1918), he used the momentum theory but adding an empirical approach like the one adopted by Drzewiecki.

A. Fage and H. E. Collins (1917), exploited the momentum theory, but with an aspect ratio like 6, the problem lay in the fact that, it was necessary to make specific corrections on the induced speed due to the variations of aspect ratio.

Thanks to subsequent developments conducted by Prandtl, a clear formulation was provided that allows to understand the effect of the induced speed determined by the wake. It was shown that the circuit around the aerodynamic profile determines the lift.

The Vortex Theory allows to incorporate the speed induced in the blade element theory. It is specified that both the previous theory and the momentum theory used a model called actuator disk.

With the blade element theory, the aerodynamic profile formulation is applied to the rotor, with the influence of the wake expressed in an induced angle of attack. The application of theory requires the estimation of the induced velocity, obtainable through the momentum theory or vortex theory.

The following points are the substantial differences that distinguish the two theories just mentioned:

- The theory of the moment allows us to conduct a global analysis, furthermore, it must be accompanied by a further theory to obtain the complete results for the design of the rotor. Remember that in the theory of the moment the disk is included by an infinite number of blades, therefore an actuator disk and infinite aspect ratio.
- The blade element theory instead refers to the flow, the load acting on the rotor blades, and the design parameters.

By knowing thrust, angular velocity, propeller diameter, and aerodynamic characteristics of the profiles, this analysis can be used as a tool for the design of the propeller because it allows the determination of the geometric characteristics.

3.1 - Analytical treatment of the theory

The blade element theory consists of applying to a rotating blade the theory used for the wing profiles. In Figure 13 it is possible to see a typical profile and in Figure 14 the notation to be used. Figure 15 shows the element placed at a distance r from the rotational axis. The rotor is considered with infinitesimal thickness (dr). The effective speed (U), that invests the rotating element, determines an angle α with the chord, this one is the angle of attack, while ϕ, the inflow angle (or geometric angle), it is formed between the effective speed (U) and the plane of the disk, as shown in Figure 15.

It should be noted that the components of speed U are:

- Tangential speed: Ωr
- Axial speed: $(V_i + V_C)$, V_C in the case of vertical flight

The speed V_c is considered in the driven propeller (propeller 2), because it has a feed speed perpendicular to the airflow.

Figure 16 represents a view from the top of the rotor, it allows to identify the radius immediately at the tip of the blade and the rotation speed with the corresponding direction of rotation.

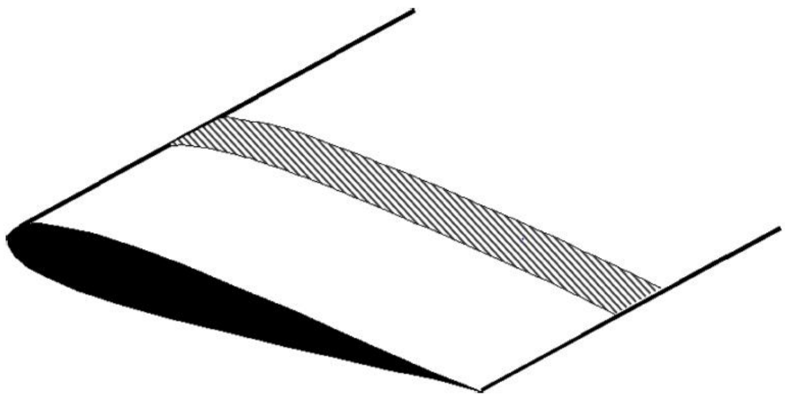

Figure 13 - Blade section

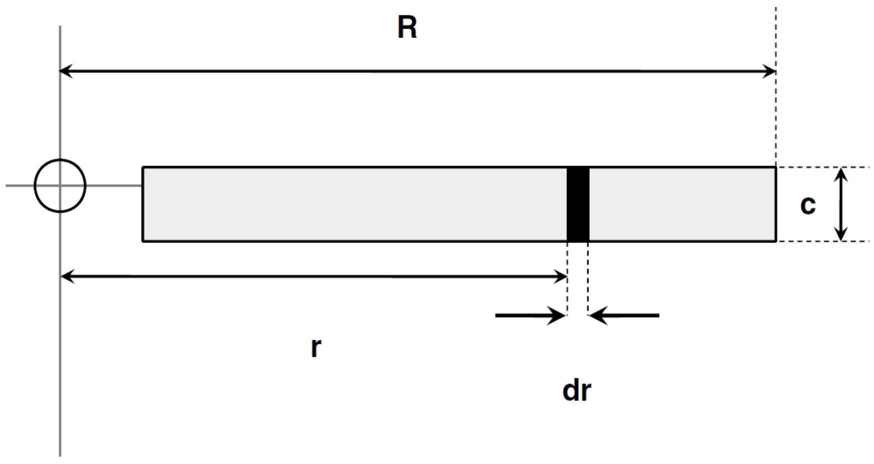

Figure 14 - Blade coordinates

$$U = \sqrt{V_i^2 + (\Omega r)^2} \tag{3.1}$$

$$\phi = \operatorname{atan}\left[\frac{V_i}{\Omega r}\right] \tag{3.2}$$

$$\alpha = \theta - \phi \tag{3.3}$$

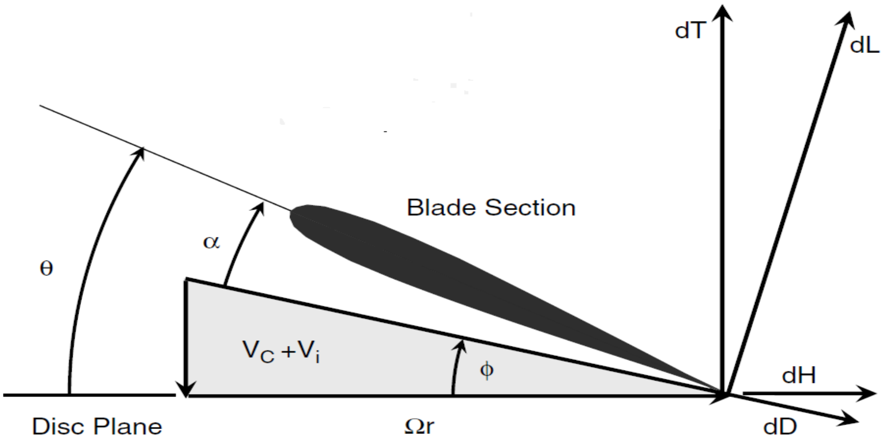

Figure 15 - Blade section characteristics

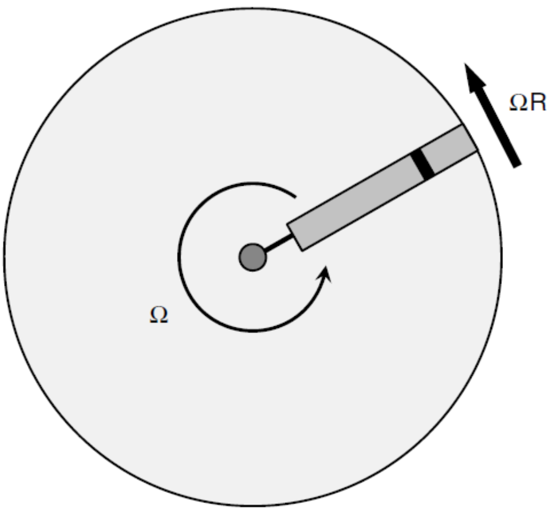

Figure 16 - Plan view

In the case of vertical flight or hover, the problem lies in the distribution of the forces shown in Figure 15, for this reason, it is necessary to integrate and then highlight the terms dependent on the radius:

$$dL = \frac{1}{2} \cdot \rho \cdot U^2 \cdot c \cdot C_L \cdot dr \tag{3.4}$$

$$dD = \frac{1}{2} \cdot \rho \cdot U^2 \cdot c \cdot C_D \cdot dr \tag{3.5}$$

$$dT = dL \cdot \cos\phi - dD \cdot \sin\phi \tag{3.6}$$

$$dQ = (dL \cdot \sin\phi + dD \cdot \cos\phi)r \tag{3.7}$$

$$dH = \frac{dQ}{r} \tag{3.8}$$

It is necessary to report some simplifications:

- The blade is assumed rigid thanks to the action of the centrifugal force.
- The inflow angle (ϕ) is assumed small, in particular, this statement is very close to reality when is considered a condition far from the axis of rotation thanks to the fact that Ωr is very high, this statement is inconsistent close to the rotation axis, even if the acting forces are small:

$$U \cong \Omega \cdot r \tag{3.9}$$

$$\cos\phi \cong 1; \sin\phi \cong \phi \tag{3.10}$$

$$\phi \cong \frac{V_i}{\Omega r} \tag{3.11}$$

Now the first equations can be rewritten with the simplification introduced:

$$dL \cong dT = \frac{1}{2}\rho\,(\Omega \cdot r)^2 C_l \cdot c \cdot dr \tag{3.12}$$

$$dQ \cong \frac{1}{2}\rho\Omega^2 r^3 (C_l\phi + C_d)c \cdot dr \tag{3.13}$$

The equation below (3.14), express the power request to the blade:

$$dP = \frac{1}{2}\rho\,(\Omega \cdot r)^3 (C_l\phi + C_d)c \cdot dr \tag{3.14}$$

If it is introduced the number of blades and the single blade has a finite size, it is necessary to integrate the equations from the inner radius to the outer. These equations represent the total physical quantities:

$$T = \frac{N \cdot \Omega^2\,\rho}{2}\int_0^R C_l \cdot c \cdot r^2 dr \tag{3.15}$$

$$Q = \frac{N \cdot \Omega^2 \cdot \rho}{2}\int_0^R (C_l\phi + C_d)c \cdot r^3 dr \tag{3.16}$$

$$P = \frac{N \cdot \Omega^3 \cdot \rho}{2}\int_0^R (C_l\phi + C_d)c \cdot r^3 dr \tag{3.17}$$

The equations below, (3.18), (3.19), (3.20) are adimensional:

$$C_T = \frac{\pi^2 T}{4 \cdot \rho \cdot \Omega^2 R^4} \tag{3.18}$$

$$C_Q = \frac{\pi^2\, Q}{8\, \rho \Omega^2 R^5} \tag{3.19}$$

$$C_P = \frac{\pi^3 P}{4 \cdot \rho \cdot \Omega^3 R^5} \tag{3.20}$$

In the Blade Element Theory is contained a parameter relative to the area of the disc, it represents the solidity (J. Seddom, 2011):

$$s = \frac{N \cdot c \cdot R}{\pi \cdot R^2} = \frac{N \cdot c}{\pi \cdot R} \tag{3.22}$$

Two other factors of fundamental importance are:

- The performance of the propeller
- The factor of merit.

In particular, the efficiency is directly proportional to the speed of ascent, so in the case of a rotor analysis in hovering, this term is useless; the merit factor, on the other hand, can have a value between 1 and 0 and is directly proportional to the induced axial speed.

$$F.M. = \frac{\int_R \; v_i \; dT}{\int_R \; \Omega \; dQ} \tag{3.23}$$

$$\sigma = \frac{N\; c(r)}{\pi \cdot R} \tag{3.24}$$

With the equations related to the coefficients introduced previously and the definition of solidity, it is possible to rewrite the coefficients as:

$$C_T = \frac{\pi^3}{8R^3} \int_0^R C_l \sigma r^2 dr \tag{3.25}$$

$$C_Q = \frac{\pi^3}{16\, R^4} \int_0^R (C_l\, \phi + C_d) \sigma r^3 dr \tag{3.26}$$

$$C_P = \frac{\pi^4}{8R^4} \int_0^R (C_l\, \phi + C_d) \sigma r^3 dr \tag{3.27}$$

4 – Vortex Theory

The vortex theory exploits the concept of actuator disk as already mentioned in the previous chapter (Blade Element Theory), the disk, made up of an infinite number of blades, is permeable and distributes the vorticity uniformly, moreover, in this theory the contraction of the wake is neglected.

The leading scholars who developed and perfected the Vortex Theory are:

- N. E. Joukowski (1912): he studied the speed induced by the helical vortex system of an actuator disk.
- Betz (1919): he determines the optimal circulation distribution on the rotor in the case of an infinite number of blades and the minimum induced power.
- L. Prandtl (1920): he developed the theory to take into consideration the circulation of a finite number of blades.
- S. Goldenstein (1929): introduced an exact correction to consider the presence of a finite number of blades.
- H. Glauert (1934): he reworked the work done by Betz in the condition of a weakly loaded disk extending the treatment to any load condition.

The Vortex Theory allows to analyze the flow field near the disk and in the wake that is generated from it under the hypothesis of inviscid and incompressible fluid.

The laws necessary for the analysis are:

- Kutta-Joukowski theorem:

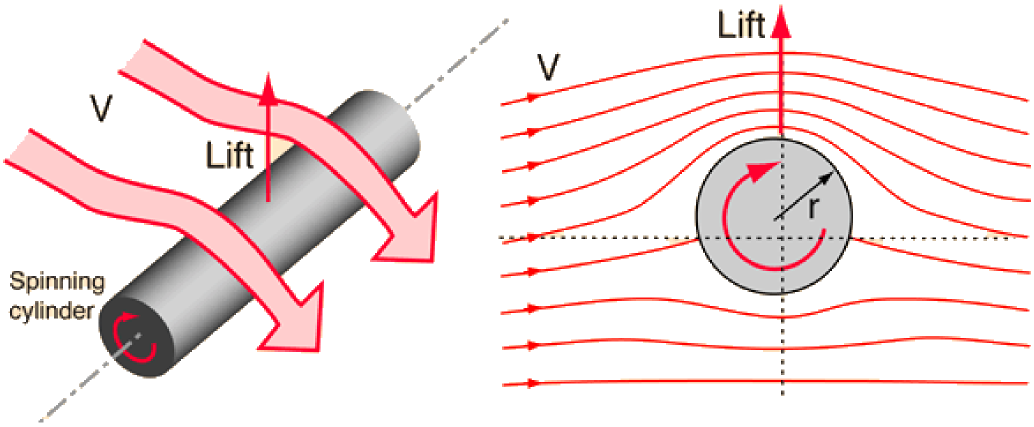

Figure 17 - Kutta - Joukowski

"*If an irrotational two-dimensional fluid current, having at infinity the velocity V_∞ surrounds any closed contour on which the circulation of velocity is Γ, the force of the aerodynamic pressure acts on this contour in a direction perpendicular to the velocity and has the value*" (J. D. Anderson, 2011).

$$L' = \rho_\infty V_\infty \Gamma_{tot} \tag{4.1}$$

- Vorticity equation:

$$\frac{D\boldsymbol{\omega}}{Dt} = \boldsymbol{\omega} \cdot \nabla \boldsymbol{V} \tag{4.2}$$

- Biot-Savar law:

In the surrounding space, a flow field is induced by the filament, moreover, if the circulation is performed in a closed path, then it has a constant value, and the term Γ represents this intensity.

$\boldsymbol{dl}$ is the vector that determines the direction of the segment, r is the distance between the segment and the point P, V is a velocity induced by the filament:

$$dV = \frac{\Gamma}{4\pi} \frac{\boldsymbol{dl} \times (\boldsymbol{r})}{|\boldsymbol{r}|^3} \tag{4.3}$$

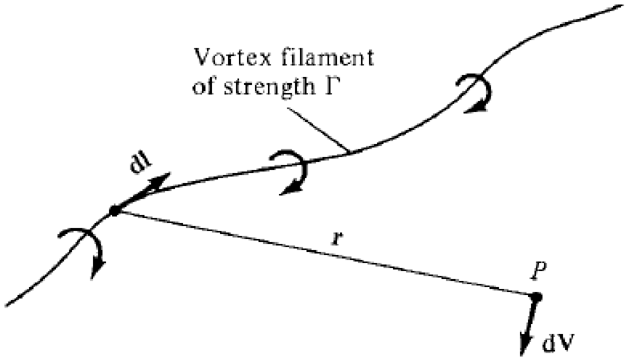

Figure 18 - Representation of the Biot Savart law

- Kelvin's theorem:

"*The time rate of change of circulation around a closed curve consisting of the same fluid elements is zero*" (J. D. Anderson, 2011).

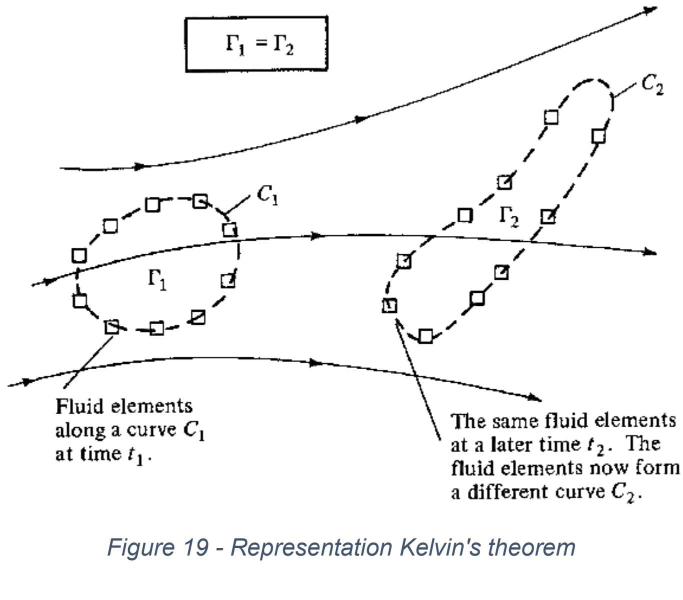

Figure 19 - Representation Kelvin's theorem

$$\frac{D}{Dt}\int_S \boldsymbol{\omega}\cdot\boldsymbol{n}\, dS = \frac{D\Gamma}{Dt} = 0 \qquad (4.4)$$

- Helmholtz theorems:

The mathematician and physicist Hermann von Helmholtz (1821-1894) was a pioneer in the use of the vortex filament for analysis of inviscid and incompressible flow, establishing principles concerning the vortex behavior:

1. "*The strength of a vortex filament is constant along its length*".
2. "*A vortex filament cannot end in a fluid; it must extend to the boundaries of the fluid (which can be* $\pm\infty$*) or form a closed path*" (J. D. Anderson, 2011).

$$\frac{D}{Dt}(\boldsymbol{\omega}\cdot\boldsymbol{n}\, dS) = 0 \qquad (4.5)$$

After having listed all the laws considered in this theory, it is possible to proceed with the integration of the Kutta-Jukowski theorem on the radius of a single blade to determine a relationship between the circuitry and the forces acting on the disk.

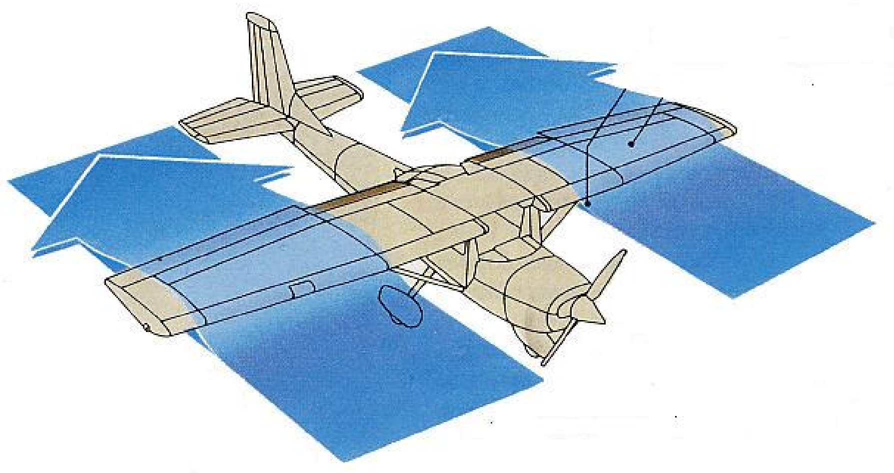

Figure 20 - Example of a wing subject to a speed flow V

$$L = \rho_\infty V_\infty \int_0^R \Gamma(r)\, dr \qquad (4.6)$$

In the case of a rotating element, the relative speed can be approximated as a product between the speed of rotation and the radius, and the elementary thrust can be considered equal to the lift; therefore, the following relation (4.7) is reported:

$$dT \cong \rho\Omega r\Gamma(r)dr \qquad (4.7)$$

Dividing by area:

$$\frac{dT}{dA} = \frac{\rho\Omega\Gamma(r)}{2\pi} \qquad (4.8)$$

Where the infinitesimal area is: $dA = 2\pi r\, dr$ and in this way, as anticipated above, a relation has been identified between thrust on area units and circulation.

4.1 – Discussion of the rotor vortex and its wake

Considering a rotor made by a finite number of blades and having a constant circulation distribution, it is possible to assume the blade equal to a whirling filament that starts from the infinite and ends at the root, moreover, the vortex filament is set on the axis of the rotor, there is also a swirling end filament, which takes on a helical shape due to the rotation of the disk and the axial velocity also determined by the disk (Figure 21)

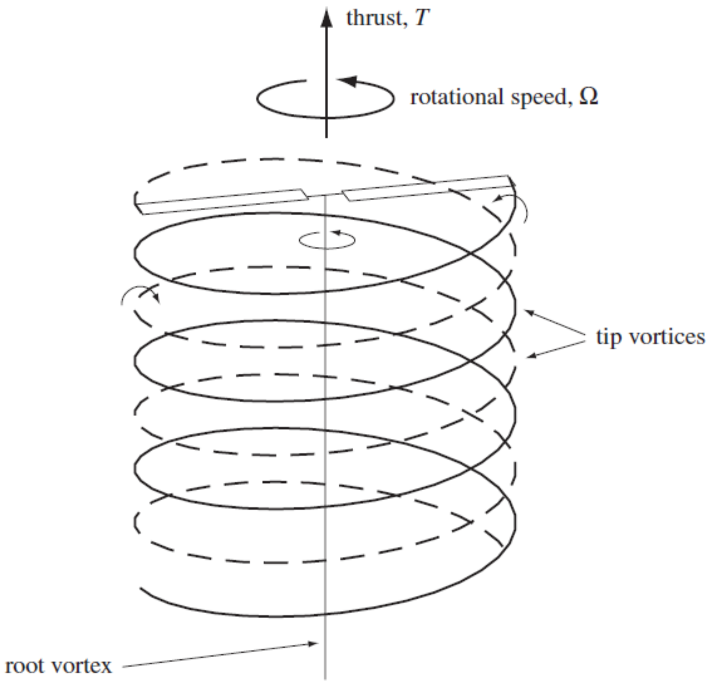

Figure 21 - Helicoidal motion

The flux is irrotational at infinity upstream of the flow tube, therefore $\boldsymbol{\omega} = 0$, passing to the two following stations "2" and "3" (the stations that enclose the rotor, Figure 9), the flow becomes rotational, in particular, the axial speed is constant, while the tangential speed undergoes an increment, passing from the null value to a finite value:

$$u(r) = \frac{\Gamma}{2\pi r} \tag{4.9}$$

Concerning the case reported, due to the uniform distribution of vorticity and vortex adhering to the blade, the root and terminal vortex, have a constant circuit value.

From equation (4.8), it is possible to determine the ratio between the thrust, the surface, and the value of the circuit (equations (4.10) and (4.11)).

$$\frac{T}{A} = \frac{\rho\Omega\Gamma}{2\pi} \tag{4.10}$$

$$\Gamma = \frac{T}{A}\frac{2\pi}{\rho\Omega} \tag{4.11}$$

The points that characterize the whirling system are listed below:

- Whirling filament aligned with the axis of the rotor having a circulation intensity equal to the equation (4.11) described.
- On the surface of the actuator disk there is a radial distribution of vortex filaments having a density:

$$\gamma_b = \frac{\Gamma}{2\pi r} \tag{4.12}$$

- The flow tube is made up of swirling rings parallel to the plane of the propeller; the rings constitute the lateral surface of the tube.
- Axial distribution and perpendicular to the whirling rings have the following intensity:

$$\gamma_l = \frac{\Gamma}{2\pi r} \tag{4.13}$$

This breakdown of the motion field was carried out in such a way as to simplify the analysis of the induced motion field.

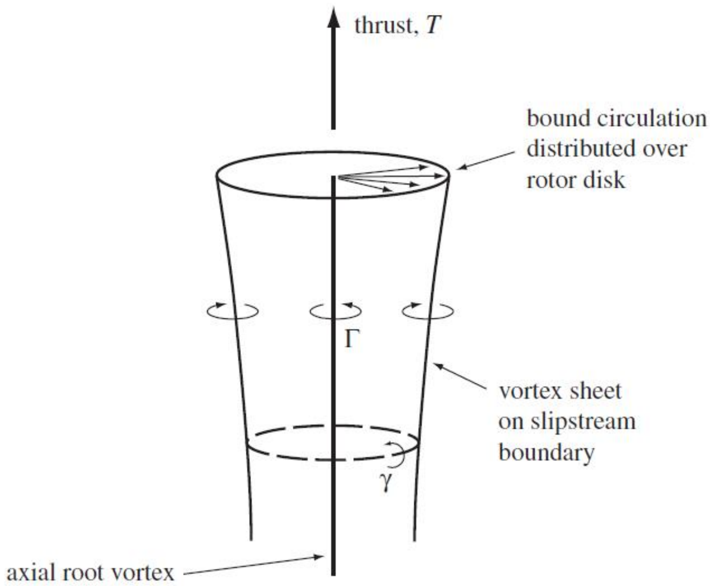

Figure 22 - Vortex theory for the actuator disk model.

The longitudinal filaments and the root vortex present in the following system do not induce any axial velocity, but determine only the rotary motion of the flow, in particular, the tangential velocity caused by the root vortex is:

$$u_{RV} = \frac{\Gamma}{4\pi r} \tag{4.14}$$

The radial vorticity distribution helps to determine the two tangential velocities below, and above the disk, they have the same form but different sign. Considering that the flow before crossing the disk is irrotational, then the velocity above the disk: $-u_b$ is opposite and equal in form to the velocity that gush from the root vortex (4.9). It is possible to determine the relations relative to the velocity below the disc (4.15) and the velocity to the infinity downstream (4.16).

$$u(r) = 2 \cdot u_{RV} = \frac{\Gamma}{2\pi r} \tag{4.15}$$

$$u_\infty(r) = u_{RV} = \frac{\Gamma}{4\pi r} = \frac{u(r)}{2} \tag{4.16}$$

The elements that allow the determination of the axial speed are the rings that make up the lateral surface of the flow tube; they have an intensity:

$$\gamma_r = \frac{\Gamma}{h} \tag{4.17}$$

The parameter h represents the distance between the whirling rings.

$$h = \frac{2\pi}{\Omega} v_i \tag{4.18}$$

In equation (4.18), v_i represents the induced axial velocity, replacing this equation in (4.17), it is obtained:

$$\gamma_r = \frac{T}{A\rho v_i} \tag{4.19}$$

Considering what reported on page 6 of (M. Knighr, 1937), it is shown that a distribution of rings, belonging to the surface of a flow tube (with density reported in equation (4.17)), determines a potential velocities in a generic point P :

$$\phi_p = \frac{\frac{d\Gamma}{dz}}{4\pi} \int_{z_1}^{z_2} \omega \, dz \tag{4.20}$$

It should be noted that z_1 and z_2 represent the extremes of integration. ω in equation (4.19) represents the solid angle subtended by the rotor; this angle is also reported in (Johnson W. , 2013), but with another symbology.

By deriving the potential concerning the variable z, the induced velocity is obtained as:

$$v_i(P) = \frac{\gamma_r}{4\pi} \int_{\omega_1}^{\omega_2} d\omega \tag{4.21}$$

Considering that the density is explained by (4.19) and the angle subtended from the ring to the downstream infinity is zero, by appropriately manipulating, the induced speed is obtained:

$$v_i(P) = \sqrt{\frac{2 \cdot T}{\pi \rho D^2}} \tag{4.21}$$

Manipulating these relations, in particular following the procedure reported in (Johnson W. , 1994), it is shown that the speed of a point placed at the infinity downstream is: $v_\infty = 2v_i$.

Therefore with this theory, the results obtained for the Simple Impulsive Theory have been confirmed.

4.1.1 – Variable distribution of $\Gamma(r)$

Considering a variable circuitry distribution, for each variation of circuiting, there is the detachment of a filament from the blade (Figure 23).

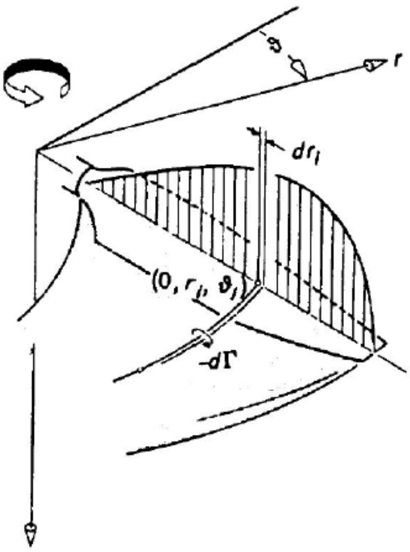

Figure 23 - Separation of the swirling filament

The set of filaments forms a swirling free surface of helical shape, as in Figure 24.

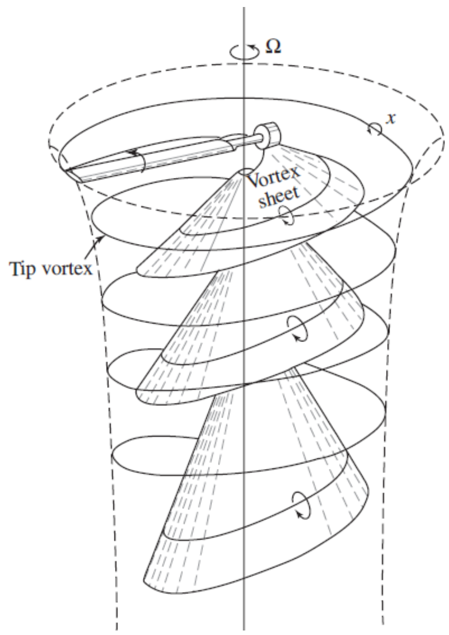

Figure 24 - Vortex sheet

Between the plane of the disk and the surfaces shown in Figure 24, an angle is formed:

$$\phi = \arctan\left(\frac{v_i}{\Omega r - \frac{u}{2}}\right) \tag{4.22}$$

Compared to the previous case with constant circuitry, in this case, considering a variable circulation and an infinite number of blades, the swirling surfaces are separated by an infinitesimal distance, and the vorticity is no longer concentrated only in the lateral surface of the flow tube but throughout the wake.

It is possible to consider the model as reported in Figure 21, so the problem is simplified.

For the Kelvin theorem, the generic filament has an intensity equal to:

$$-\frac{d\Gamma(r)}{dr} \tag{4.23}$$

In particular, the density of the whirling rings is:

$$\gamma(r) = -\frac{d\Gamma(r)}{dr}\cdot\frac{1}{h} = -\frac{d\Gamma(r)}{dr}\cdot\frac{\Omega}{2\pi v_i} \tag{4.24}$$

As far as the determination of the tangential speed is concerned, it has a relation equal to that shown in (4.15), with the circulation variable according to the radius.

Applying Bernoulli's law to the current lines, the pressure increase across the disc takes into account the tangential speed and axial speed:

$$\Delta p = \rho \left(2v_i^2 - \frac{u^2}{2} \right) \quad (4.25)$$

It is also possible to evaluate the elementary thrust (4.26) and compare it with the thrust obtainable by the Kutta-Jukowski law (4.27), obtaining the variable circuitry as a function of the induced speed.

$$dT = 2\pi\rho \left(2v_i^2 - \frac{u^2}{2} \right) \quad (4.26)$$

$$dT = \rho V_e \Gamma dr = \rho \left(\Omega r - \frac{u}{2} \right) \Gamma dr \quad (4.27)$$

$$\Gamma(r) = \frac{4\pi v_i^2}{\Omega} \quad (4.28)$$

Equation (4.28) is determined by equating (4.26) and (4.27).

4.2 - Optimal vortex system

As demonstrated by Betz, a weakly charged propeller, the condition of minimum induced energy requires that the vortex surface must rotate around the rotation axis, as a rigid surface, and form with the disk plane a constant angle for each dimension (ϕ). Then the swirling surface can be assimilated to an Archimedean screw.

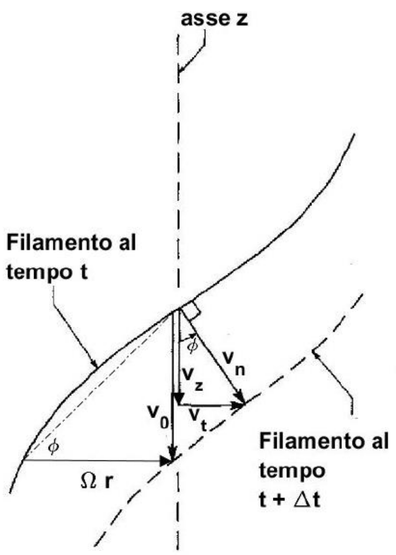

Figure 25 – Rotor wake

The Archimedean screw, which is formed by the swirling trail, pushes the fluid downstream. As shown in Figure 25, three velocity components are formed: perpendicular to the vortex trail (v_n), one directed along the rotation axis (v_z), and the last tangential (v_t). The speed of the wake relative to the disc is constant and is v_0. To determine the three indicated speeds, they are expressed as a function of angle ϕ and speed v_0:

$$v_n = v_0 \cdot \cos\phi \tag{4.29}$$

$$v_t = v_0 \cdot cos\phi \cdot \sin\phi \tag{4.30}$$

$$v_z = v_0 \cos^2\phi \tag{4.31}$$

The ϕ angle is:

$$\phi \cong \arctan\left(\frac{v_0}{\Omega r}\right) \tag{4.32}$$

The speed v_t is the component of v_n, while the absolute tangential speed is:

$$u = \omega r$$

In the inflow angle, it is possible to consider the climb velocity or the cruise speed, as reported in chapter 6, to describe a condition different from the hover. (4.33)

4.2.1 - Determination of the optimum circulation

As explained at the beginning of Chapter 4, Betz determined the optimal circulation distribution for a disk having an infinite number of blades and weakly loaded. Subsequently, Glauert extended this treatment to any load condition and provided a formulation and a mathematical solution of the condition problem minimum induced power and, considering the pressure variation of the Extended Impulsive Theory (equation (2.25)), the elementary thrust is determined:

$$dT = 2\pi\rho\left(\Omega r - \frac{u}{2}\right) ur\ dr \tag{4.34}$$

Considering that v_i = $\Omega\, r \tan\phi$ and $dP_i = dT\ v_i$, the induced elementary power is:

$$dP_i = 2\pi\rho\left(\Omega r - \frac{u}{2}\right) ur\ dr\ v_i = 2\pi\rho\left(\Omega r - \frac{u}{2}\right) u\Omega r^2 \tan\phi\, dr \tag{4.35}$$

Using the calculation of the variations based on the Euler-Lagrange equations, Glauert determined an equation that allows to obtain the condition of Minimum induced power of the rotor, knowing the necessary thrust, as reported in (Peters, 2016):

$$(X-1)(3X-6)^2 = \tilde{r}(3X-4)^2 \tag{4.36}$$

Making explicit:

$$X = \frac{2\Omega}{\omega} \tag{4.37}$$

$$\omega = \frac{u}{r} \tag{4.38}$$

$$\tilde{r} = \frac{r}{(RG)} \tag{4.39}$$

The parameter G indicated as v_0 in (Peters, 2016), represents a Lagrange multiplier, as explained later, it assumes an arbitrary value to obtain the maximum of the function, which in this case is the assigned value of the thrust.

The dimensionless angular velocity is:

$$\bar{\omega} = \frac{\omega}{\Omega} = \frac{2}{X} \tag{4.40}$$

$$\bar{\omega} = \frac{6}{5 + \tilde{r}^2 + 2(1 + \tilde{r}^2)\cos\left(\frac{\theta}{3}\right)} \tag{4.41}$$

θ is calculated as:

$$\theta = \arccos\left(\frac{\tilde{r}^6 + 3\tilde{r}^4 + 3\tilde{r}^2 - 1}{\tilde{r}^6 + 4\tilde{r}^4 + 3\tilde{r}^2 + 1}\right) \tag{4.42}$$

Explaining the circuit as a function of the radius from equation (4.15) and replacing the tangential speed $u = \omega r = \bar{\omega}\Omega r$, it is possible to obtain:

$$\Gamma(r) = 2\pi r^2 \bar{\omega}\Omega \tag{4.43}$$

The dimensionless circulation is derived from the latter, and the typical trend is reported in Figure 26.

$$\bar{\Gamma}(r) = \frac{\Gamma(r)}{2\pi\Omega R^2 G^2} = \bar{\omega}\left(\frac{r}{RG}\right)^2 \tag{4.44}$$

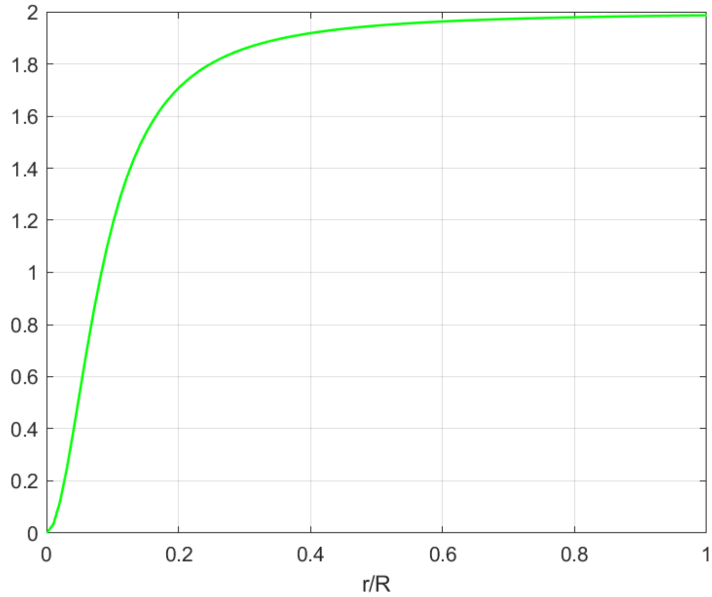

Figure 26 - Adimentional circulation

4.2.2 – Prandtl correction

In the case of the finite number of blades, energy losses occur, caused by the motion of the fluid, which escapes from the helical vortex surface and flows around the edge of the upper and lower face causing a reduction in the axial momentum.

In the case of an infinite number of blades, this phenomenon did not occur thanks to the presence of contiguous swirling surfaces, which hindered this phenomenon.

The phenomenon, exposed later analytically, occurs with the cancellation of lift and circulation to the tip of the blades.

Glauert made an equation that allowed simple evaluation of tip losses for the BEM (Blade Element Theory) model, thus exploiting a two-dimensional model Glauert obtained a factor that multiplied by the circulation approximates the effects of such losses. This discussion is also presented in (Sørensen, 2016)

$$F(r) = \frac{2}{\pi} \arccos(e^{-f}) \tag{4.45}$$

$$f = \frac{N}{2} \cdot \frac{(R-r)}{r\phi} \tag{4.46}$$

In equation (4.46), N represents the number of blades, while ϕ is the inflow angle exposed above. By tracing the behavior of the Prandtl factor with the variation of the number of blades as in Figure 27, it is possible to see how at the tip (as the number of blades increases) F tends to the unit value.

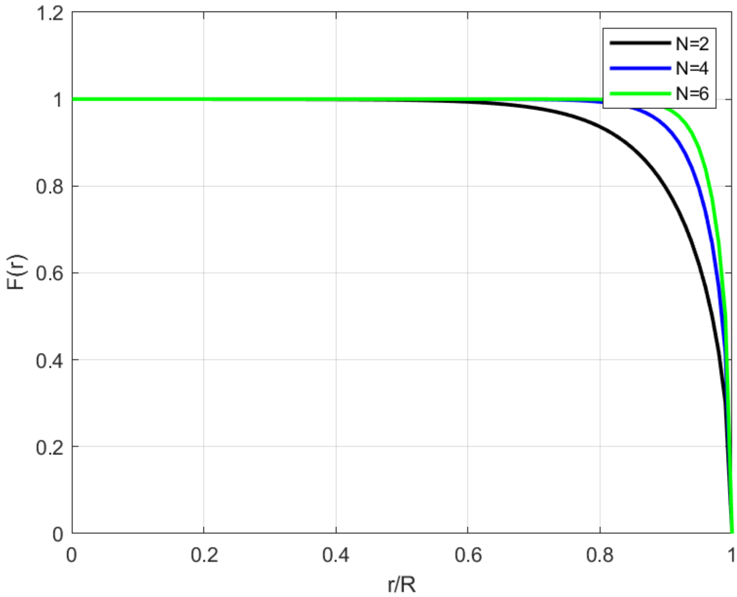

Figure 27 - Prandtl factor

Once the Prandtl factor has been determined, it is possible to correct the adimensional circuitry determined for an infinite number of blades; the correction consists in introducing both the energy losses to the tip and the finite number of blades which in this case is equal to 2 ($N = 2$).

$$\bar{\Gamma}_c(r) = F(r)\overline{\omega}\left(\frac{r}{RG}\right)^2 = \frac{2}{\pi}\arccos\left(e^{\frac{(r-R)}{r\phi}}\right)\overline{\omega}\left(\frac{r}{RG}\right)^2 \tag{4.47}$$

The problem related to the resolution of equation (4.47) is correlated to the presence of two free parameters which are v_0, contained in ϕ, and the load parameter G. One of the two can be eliminated by imposing the thrust, moreover, it needs to add a relation that links v_0 and G. The first term has the dimensions of speed, while the load parameter is adimensional.

Through the properties of the trigonometric functions, it is possible to derive the equation (4.48) from (4.30):

$$v_t = \frac{v_0^2\ \Omega r}{(\Omega r)^2 + v_0^2} \tag{4.48}$$

$$u = 2\frac{v_0^2 \Omega r}{(\Omega r)^2 + v_0^2} \tag{4.49}$$

The (4.49) has been obtained considering that $u = 2 \cdot v_t$ and knowing that $u = \omega \cdot r = \overline{\omega}\Omega r$ ($\overline{\omega}$ is a function of G as shown by the equation (4.41))

$$u = \Omega r\ \overline{\omega}(G) \tag{4.50}$$

$$\overline{\omega}(G) = \frac{2v_0^2}{(\Omega r)^2 + v_0^2} \tag{4.51}$$

The equation (4.51) was obtained by equating (4.49) and (4.50).

The following shows the trend of the correct dimensionless circuit (Figure 28).

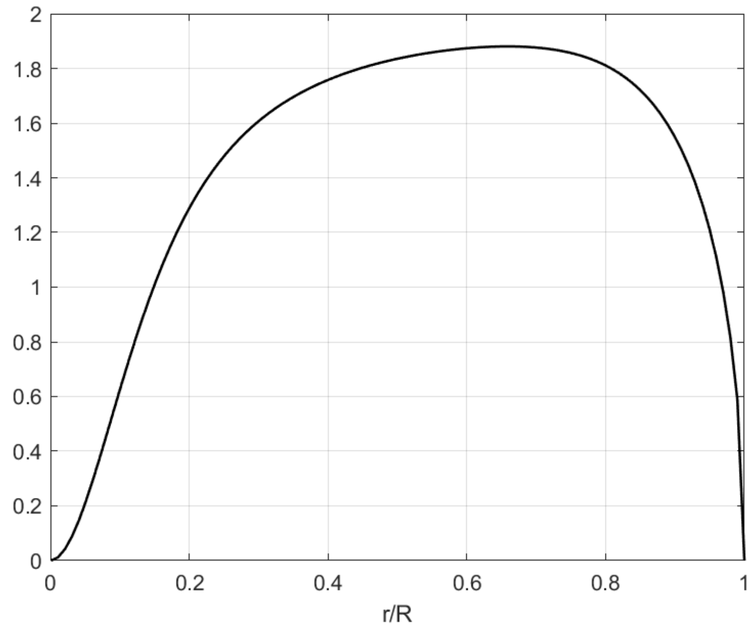

Figure 28 – Γ adimensional corrected

5 – Linearized theory of the actuator disk

5.1 – Exposition of the problem and formulation

"*Through the theory presented in (Conway, 1997), it is possible to determine more precisely the effect due to the presence of more propellers and also extends the theory of the actuator disk with radially and constant distributed load, to calculate the range of motion in all the domain considering any distribution of axial speed*" (Zazza, 2017).

For the treatment, it is considered an incompressible and rotational flow due to the intrinsic property of the propeller filed, which is a vortex region.

$$\nabla \times \boldsymbol{V} \neq 0$$

$$\nabla \cdot \boldsymbol{V} = 0$$

Thanks to the compressibility of the fluid, it is possible to define an arbitrary potential vector A that allows the representation of the motion field:

$$\boldsymbol{V} = \nabla \times \boldsymbol{A} \tag{5.1}$$

Due to the arbitrariness of the potential vector, the following condition is taken:

$$\nabla \cdot \boldsymbol{A} = 0 \tag{5.2}$$
$$\nabla^2 \boldsymbol{A} = -\boldsymbol{\omega} \tag{5.3}$$

The vector $\boldsymbol{\omega}$ represents the vorticity; as previously exposed in this treatment, it is different from 0, and the problem is symmetrical. Therefore the vector $\boldsymbol{\omega}$ is written as a function of the derivatives reported in equation (5.4).

$$\boldsymbol{\omega} = \nabla \times \boldsymbol{V} = (\omega_r, \omega_\theta, \omega_z) = \left(-\frac{\partial v_\theta}{\partial z}, \frac{\partial v_r}{\partial z} - \frac{\partial v_z}{\partial r}, \frac{1}{r}\frac{\partial (r v_\theta)}{\partial r} \right) \tag{5.4}$$

Thanks to the presence of cylindrical symmetry the only non-zero component of the potential vector is A_θ, and with (5.3), which expresses the link between the potential vector and vorticity, it is possible to rewrite (5.4) eliminating the null terms

$$\boldsymbol{\omega} = (0, \omega_\theta, 0) \tag{5.5}$$

The terms: $A_\theta(r,z), v_r(r,z), v_z(r,z)$ are induced fields obtained using an axisymmetric vorticity distribution.

Equation (5.1) is expressed through the potential vector in cylindrical coordinates to obtain the velocity field.

$$V = \nabla \times A = (v_r, v_\theta, v_z) = \left(-\frac{\partial A_\theta}{\partial z}, 0, \frac{1}{r}\frac{\partial (r\, A_\theta)}{\partial r} \right) \tag{5.6}$$

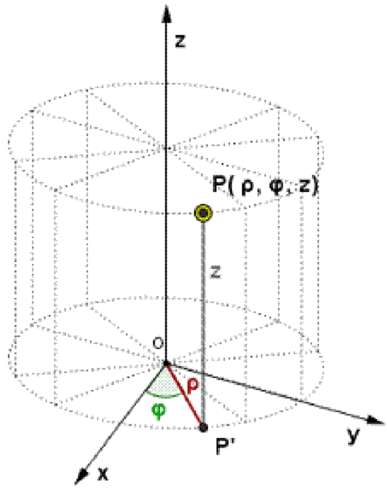

Figure 29 - Cylindrical coordinate system

Figure 29 shows a cylindrical reference system, concerning the figure, the radius ρ corresponds to r and the angle ϕ to θ.

The exposed problem is characterized by an incompressible and symmetrical flow, as explained above, so it is possible to introduce the current function $\Psi\ (r, z)$, it is linked to the velocity components through the following equations:

$$v_r = -\frac{1}{r}\frac{\partial \Psi}{\partial z} \tag{5.7}$$

$$v_z = \frac{1}{r}\frac{\partial \Psi}{\partial r} \tag{5.8}$$

From the comparison of the last two equations with the (5.6), it is possible to obtain $A_\theta = \Psi/r$, therefore replacing the (5.7) and (5.8) in the azimuthal component of the vorticity is obtained:

$$\begin{gathered} \omega_\theta = -\frac{1}{r}\frac{\partial^2 \Psi}{\partial z^2} + \frac{1}{r^2}\frac{\partial \Psi}{\partial r} - \frac{1}{r}\frac{\partial^2 \Psi}{\partial r^2} \\ \frac{\partial^2 \Psi}{\partial r^2} - \frac{1}{r}\frac{\partial \Psi}{\partial r} + \frac{\partial^2 \Psi}{\partial z^2} = -r\omega_\theta \end{gathered} \tag{5.9}$$

Equation (5.9) can also be expressed through a linear differential operator

$$\mathcal{L}_{(r,z)}\left(\frac{\Psi}{r}\right) = r\left(\frac{\partial^2 \Psi}{\partial r^2} + \frac{1}{r}\frac{\partial \Psi}{\partial r} - \frac{\Psi}{r^2} + \frac{\partial^2 \Psi}{\partial z^2}\right)\frac{1}{r} = -r\omega_\theta \tag{5.10}$$

The (5.10) represents the governing law of the motion field determined by an axial vorticity distribution $\left(\omega_\theta(r, z)\right)$. The equation (5.10) represents the beginning of the study related to the determination of the flow induced by an immersed propeller in an ideal fluid. It is necessary to impose the following boundary conditions to solve the equation (5.10).

$$v_z = \frac{1}{r}\frac{\partial \Psi}{\partial z} \to 0$$
$$v_r = -\frac{1}{r}\frac{\partial \Psi}{\partial z} \to 0 \; if \; r \to \infty \;\; or \; z \to \pm\infty \tag{5.11}$$

To determine the induced speed field, proceed from the equation (5.10) and consider a single whirling ring. In particular, in chapter 6, the axial velocity distribution and tangential velocity distribution are calculated.

5.1.1 – Problem solution

The solution to the problem is determined by referring to a vortex ring of intensity Γ, it determines a potential vector $A_\theta(r,z)$ and a motion field identified by the successive equations; the following treatment is also reported in (Besset, 1888):

$$A_\theta(r,z) = \frac{\Psi(r,z)}{r} = \frac{\Gamma\sigma}{2}\int_0^\infty J_1(s\sigma)J_1(sr)e^{-s|z-\zeta|}ds \tag{5.12}$$
$$v_r(r,z) = \frac{\Gamma\sigma}{2}\int_0^\infty sJ_1(s\sigma)J_1(sr)e^{-s|z-\zeta|}ds \quad if \; z \geq \zeta \tag{5.13}$$
$$v_r(r,z) = -\frac{\Gamma\sigma}{2}\int_0^\infty sJ_1(s\sigma)J_1(sr)e^{-s|z-\zeta|}ds \quad if \; z < \zeta \tag{5.14}$$
$$v_z(r,z) = \frac{\Gamma\sigma}{2}\int_0^\infty sJ_1(s\sigma)J_0(sr)e^{-s|z-\zeta|}ds \tag{5.15}$$

The surface density in the considered domain is introduced, it is possible to reformulate the equations just described and to consider them concerning more whirling rings rather than one. By introducing the density, the domain can be extended along z to all values greater than 0; while the radius r, it can vary from 0 to the reference R; the determination of the radius R is shown in the next chapter.

$$A_\theta(r,z) = \frac{\Psi(r,z)}{r} = \frac{1}{2}\int_0^\infty\int_0^{R(z)}\int_0^\infty \gamma(\sigma,\zeta)\sigma\, J_1(s\sigma)\, J_1(sr)\, e^{-s|z-\zeta|}ds d\sigma d\zeta \tag{5.16}$$
$$v_r(r,z) = \frac{1}{2}\int_0^\infty\int_0^{R(z)}\int_0^\infty \gamma(\sigma,\zeta)\sigma\, s\, J_1(s\sigma)\, J_1(sr)\, e^{-s|z-\zeta|}ds d\sigma d\zeta \quad if \; z \geq \zeta \tag{5.17}$$
$$v_r(r,z) = \frac{1}{2}\int_0^\infty\int_0^{R(z)}\int_0^\infty -\gamma(\sigma,\zeta)\sigma\, s\, J_1(s\sigma)\, J_1(sr)\, e^{-s|z-\zeta|}ds d\sigma d\zeta \quad if \; z < \zeta \tag{5.18}$$
$$v_z(r,z) = \frac{1}{2}\int_0^\infty\int_0^{R(z)}\int_0^\infty \gamma(\sigma,\zeta)\sigma\, s\, J_1(s\sigma)\, J_0(sr)\, e^{-s|z-\zeta|}ds d\sigma d\zeta \tag{5.19}$$

In the equations just described, the vorticity density and the radius R are not known, to determine the density the Vortex Theory is used, while as regards R, it varies along z. To eliminate the contraction, R is assumed constant to linearize the exposed treatment.

For the vorticity density, the equation (5.20) is considered, it is possible to see that it depends only on the coordinate r, while v_i represents the induced axial velocotà.

$$\gamma(\sigma) = -2\frac{dv_i(\sigma)}{d\sigma} \tag{5.20}$$

With the simplifications introduced, the equations (5.16), (5.17), (5.18), and (5.19) are rewritten, modifying the integration extreme eliminating the dependence on the z dimension.

$$A_\theta(r,z) = \frac{\Psi(r,z)}{r} = \frac{1}{2}\int_0^\infty \int_0^R \int_0^\infty \gamma(\sigma)\sigma\, J_1(s\sigma)\, J_1(sr)\, e^{-s|z-\zeta|} ds d\sigma d\zeta \tag{5.21}$$

$$v_r(r,z) = \frac{1}{2}\int_0^\infty \int_0^{R(z)} \int_0^\infty \gamma(\sigma)\sigma\, s\, J_1(s\sigma)\, J_1(sr)\, e^{-s|z-\zeta|} ds d\sigma d\zeta \quad if\ z \geq \zeta \tag{5.22}$$

$$v_r(r,z) = \frac{1}{2}\int_0^\infty \int_0^{R(z)} \int_0^\infty -\gamma(\sigma)\sigma\, s\, J_1(s\sigma)\, J_1(sr)\, e^{-s|z-\zeta|} ds d\sigma d\zeta \quad if\ z < \zeta \tag{5.23}$$

$$v_z(r,z) = \frac{1}{2}\int_0^\infty \int_0^{R(z)} \int_0^\infty \gamma(\sigma)\sigma\, s\, J_1(s\sigma)\, J_0(sr)\, e^{-s|z-\zeta|} ds d\sigma d\zeta \tag{5.24}$$

By integrating concerning the variable ζ, which represents the center of the ring in the z-axis, the speeds concerning r and z become:

$$v_r(r,z) = \int_0^R \int_0^\infty \frac{dv_i(\sigma)}{d\sigma}\, \sigma\, J_1(s\sigma) J_1(sr) e^{-s|z|} ds d\sigma \tag{5.25}$$

$$v_z(r,z) = -\int_0^R \int_0^\infty \frac{dv_i(\sigma)}{d\sigma}\, \sigma\, J_1(s\sigma) J_0(sr)\left(2 - e^{-s|z|}\right) ds d\sigma \quad if\ z \geq 0 \tag{5.26}$$

$$v_z(r,z) = -\int_0^R \int_0^\infty \frac{dv_i(\sigma)}{d\sigma}\, \sigma\, J_1(s\sigma) J_1(sr) e^{-s|z|} ds d\sigma \quad if\ z < 0 \tag{5.27}$$

Evaluating the equation (5.26) in $z = 0$:

$$v_z(r,0) = -\int_0^R \int_0^\infty \frac{dv_z(\sigma,0)}{d\sigma}\, \sigma\, J_1(s\sigma) J_0(sr) ds d\sigma \tag{5.28}$$

Placing $v_z(\sigma,0) = f(\sigma)$ and changing the integral extremes concerning $d\sigma$

$$v_z(r,0) = -\int_0^\infty \int_0^\infty f'(\sigma)\, \sigma\, J_1(s\sigma) J_0(sr) ds d\sigma \tag{5.29}$$

The equation (5.30) shows the first-order Henkel transform obtained from $f'(\sigma)$ of equation (5.29)

$$G_1(s) = H_1\left(f'(\sigma)\right) = \int_0^\infty f'(\sigma)\, \sigma\, J_1(s\sigma)\, d\sigma \tag{5.30}$$

$$F_0(s) = H_0\left(f(\sigma)\right) = \int_0^\infty f(\sigma)\, \sigma\, J_0(s\sigma)\, d\sigma \tag{5.31}$$

The (5.31) is the Henkel transform of zero order. For the properties of the Henkel function, it is possible to obtain:

$$G_1(s) = H_1\left(f'(\sigma)\right) = -sF_0(s) \tag{5.32}$$

$$\int_0^\infty f'(\sigma)\, \sigma\, J_1(s\sigma)\, d\sigma = \int_0^\infty -f(\sigma)\, s\sigma\, J_0(s\sigma)\, d\sigma \tag{5.33}$$

Considering that this relation must be satisfied for all $\sigma \geq 0$, it is obtained:

$$f'(\sigma)\,\sigma\, J_1(s\sigma) = -f(\sigma)\, s\sigma\, J_0(s\sigma) \tag{5.34}$$

Replacing the (5.34) equation in (5.25), (5.26) and (5.27), the velocities are functions of the axial one.

$$v_r(r,z) = -\int_0^R \int_0^\infty v_z(\sigma,0) s\,\sigma\, J_0(s\sigma) J_1(sr) e^{-s|z|} ds d\sigma \tag{5.35}$$

$$v_z(r,z) = \int_0^R \int_0^\infty v_z(\sigma,0) s\,\sigma\, J_0(s\sigma) J_0(sr)\left(2 - e^{-s|z|}\right) ds d\sigma \;\; if\; z \geq 0 \tag{5.36}$$

$$v_z(r,z) = \int_0^R \int_0^\infty v_z(\sigma,0) s\,\sigma\, J_0(s\sigma) J_0(sr) e^{-s|z|}\; ds d\sigma \;\; if\; z < 0 \tag{5.37}$$

Separating (5.36) into two integrals:

$$v_z(r,z) = I_1 - I_2 = 2\int_0^R \int_0^\infty v_z(\sigma,0) s\,\sigma\, J_0(s\sigma) J_0(sr) ds d\sigma - \int_0^R \int_0^\infty v_z(\sigma,0) s\,\sigma\, J_0(s\sigma) J_0(sr)\left(e^{-s|z|}\right) ds d\sigma \tag{5.38}$$

Manipulating the last equation, the (5.39) is obtained:

$$I_1 = 2\int_0^\infty v_z(\sigma,0)\,\sigma \left[\int_0^\infty s J_0(s\sigma) J_0(sr) ds\right] d\sigma \tag{5.39}$$

The inner integral of equation (5.39) is possibly rewritten for the property of the Bessel function:

$$\int_0^\infty s J_0(s\sigma) J_0(sr) ds = \frac{\delta(\sigma - r)}{\sigma} \tag{5.40}$$

$$I_1 = 2\int_0^\infty v_z(\sigma,0)\,\delta(\sigma - r)\, d\sigma \tag{5.41}$$

Considering the properties of delta Dirac:

$$I_1 = 2\int_0^\infty v_z(\sigma,0)\,\delta(\sigma - r)\, d\sigma = v_z(r,0) \tag{5.42}$$

Thanks to the result obtained, the equation (5.26) is simplified as follows:

$$v_z(r, z \geq 0) = 2v_z(r,0) - v_z(r, z < 0) \tag{5.42}$$

Finally, the equations of the linearized theory to be implemented are, equation (5.42) and (5.44):

$$v_r(r,z) = -\int_0^R \int_0^\infty v_z(\sigma,0) s\,\sigma\, J_0(s\sigma) J_1(sr) e^{-s|z|} ds d\sigma \tag{5.43}$$

$$v_z(r, z < 0) = \int_0^R \int_0^\infty v_z(\sigma,0) s\,\sigma\, J_0(s\sigma) J_0(sr)\left(e^{-s|z|}\right) ds d\sigma \tag{5.44}$$

6 – Propellers design

In the previous chapters, all theories used for the design of the propeller were exposed; in the following chapter are listed the results obtained, the analysis of the chosen aerodynamic profiles, and the CAD model relative to the two propellers, one necessary for take-off and one for horizontal flight.
The scenario refers to a height of 4000 m, where there are the following features:

Table 5 - Atmospheric characteristics

Temperature	$262.15\ [K]$
Pressure in ISA condition	$6.5 \cdot 10^4\ [Pa]$
Density	$0.8631\ [kg/m^3]$
Dynamic viscosity	$1.665 \cdot 10^{-5}$
Cinematic viscosity	$1.929 \cdot 10^{-5}$
Speed of sound	$324.72\ [m/s]$
Gravity acceleration	$9.81\ [m/s^2]$

The drawing up of the following paragraphs is simplified in this way, the propeller developed for take-off is called propeller 1, while the propeller for horizontal flight is propeller 2.

6.1 - Radius determination and angular velocity

After determining the atmospheric characteristics, the radius relative to the two propellers is evaluated. Below there are the equations implemented on Matlab and the choice of the thrust coefficient C_T, the following value is determined on a statistical basis by referring to a propellers database developed by the company "APC propellers":

$$C_T = \frac{\pi^2}{4} \cdot \frac{T}{\rho V_{tip}^2 R^2} \tag{6.1}$$

The equation (6.1) is equal to (3.18) of chapter 3 related to the Blade Element Theory, through an inverse equation it is possible to make explicit the radius of the disk R and determine the rotation speed.

$$R = \frac{\pi}{2 \cdot V_{tip}} \sqrt{\frac{T}{\rho C_T}} \tag{6.2}$$

$$\Omega = \frac{V_{tip}}{R} \tag{6.3}$$

The values obtained for the two propellers are shown below:

- Propeller 1:
    - $C_T = 0.085$
    - $V_{tip} = 0.85 \cdot 0.5 \cdot V_s = 138\ [m/s]$
    - $R = 0.1316\ [m]$
    - $\Omega = 1048.5\ [rad/s]$

- Propeller 2.
    - $C_T = 0.065$
    - $V_{tip} = 0.85 \cdot 0.5 \cdot V_s = 179.4\ [m/s]$
    - $R = 0.2316\ [m]$
    - $\Omega = 774.78 [rad/s]$

6.2 – Application of the Vortex Theory

In the following paragraph, the results obtained from the application of Vortex Theory are explained, in particular, differentiating the case for the propeller modeled for take-off (propeller 1) and the driving propeller (propeller 2). The Skywalker X8 has a cruising speed of around 19 [m / s].

The procedure described in chapter 4 is used to determine the optimum circulation:

- The radius $\check{r}$ is determined by equation (4.39).
- Parameter θ with: (4.42).
- The dimensionless angular velocity $\overline{\omega}$: (4.41)
- The circulation: (4.34)
- The dimensionless circulation: (4.44).

6.2.1 – Infinite number of blades

In the dimensionless circulation, the Glauert load parameter is present (G), this parameter is calculated iteratively, in particular, G represents a Lagrange multiplier, and is an arbitrary parameter chosen to maximize the desired function, to determine it in the case of infinite number of blades, the following equation has been implemented:

$$T_{N_\infty} = \int_0^R dT(r) = 2\pi\rho \int_0^R \left(\Omega - \frac{\omega}{2}\right) \omega r^3 dr \tag{6.4}$$

Considering that the circulation of optimum is a function of the dimensionless angular velocity by (4.37) and the angular velocity ω can be determined as $\omega = u(r)/r$, then determining the tangential velocity from (4.36) it is possible to establish the dependence of the thrust as a function of the Glauert load parameter.

The G parameter is:

- 0.0832 for propeller 1
- 0.0457 for propeller 2.

6.2.2 – Finite number of blades

In the case of the finite number of blades, the energy losses at the tip are considered using the Prandtl parameter. The following paragraph also calculates the Glauert load parameter G because the losses were not considered in the previous paragraph.

Initially, the relative velocity between the wake and the disc is calculated:

$$v_0 = \pm\Omega r \sqrt{\frac{\bar{\omega}(G)}{2 - \bar{\omega}(G)}} \tag{6.5}$$

Another essential variable is the inflow angle (ϕ), the following angle takes into account the inclination of the wake compared to the disc, so in the case of hovering, only the speed (v_0) acts, the equation is:

$$\phi = \arctan\left(\frac{v_0}{\Omega r}\right) \tag{6.6}$$

In the case of the propeller 2, in addition to the axial speed v_0, there is the nominal cruising speed of the drone, which is about 19 $[m/s]$, so the equation (6.6) becomes:

$$\phi = \arctan\left(\frac{v_0 + V}{\Omega r}\right) \quad (6.6)$$

Once the following values have been identified, the correct optimal circulation is calculated.

A final precaution before exposing the results is relative to the thrust, which is used to determine the G factor, as shown in the previous paragraph.

$$T_{25\%} = N \cdot 2\pi \cdot \rho\Omega R^2 G^2 \int_{0.25\,R}^{R} \left(\Omega r - \frac{\bar{\Gamma}_{corr}\Omega R^2 G^2}{2r}\right) \bar{\Gamma}_{corr} dr \tag{6.7}$$

The parameters obtained are:

- 0.0983 for propeller 1
- 0.0567 for propeller 2

The thrust is considered by 25% of the radius, up to the tip, because usually, the hub is up to 25%.

Below there are the optimal circulations respect to the dimensionless circulation.

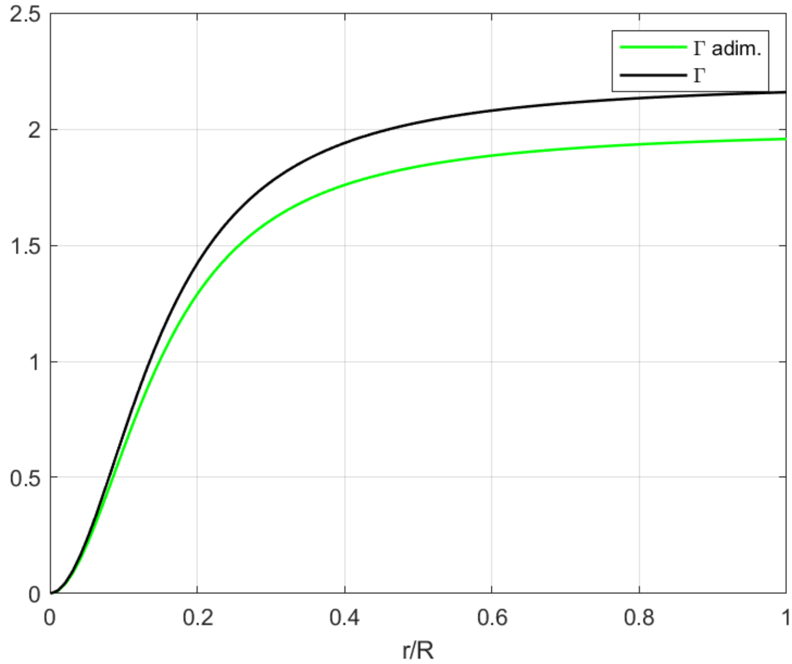

Figure 30 - Circulation for infinite number of blade (propeller 1)

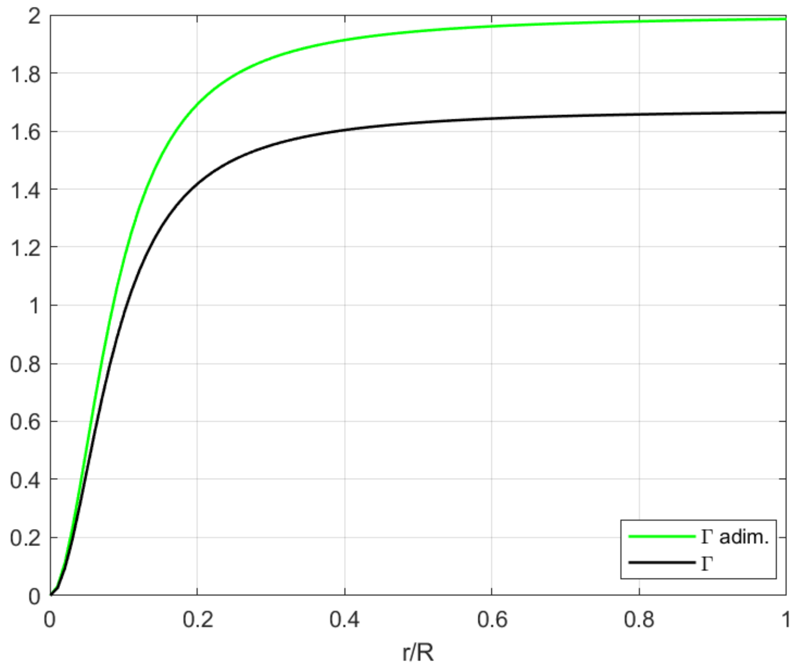

Figure 31 - Circulation for infinite number of blade (propeller 2)

In Figures 30 and 31 are reported the correct circulation taking in to account the Prandtl's factor (F).

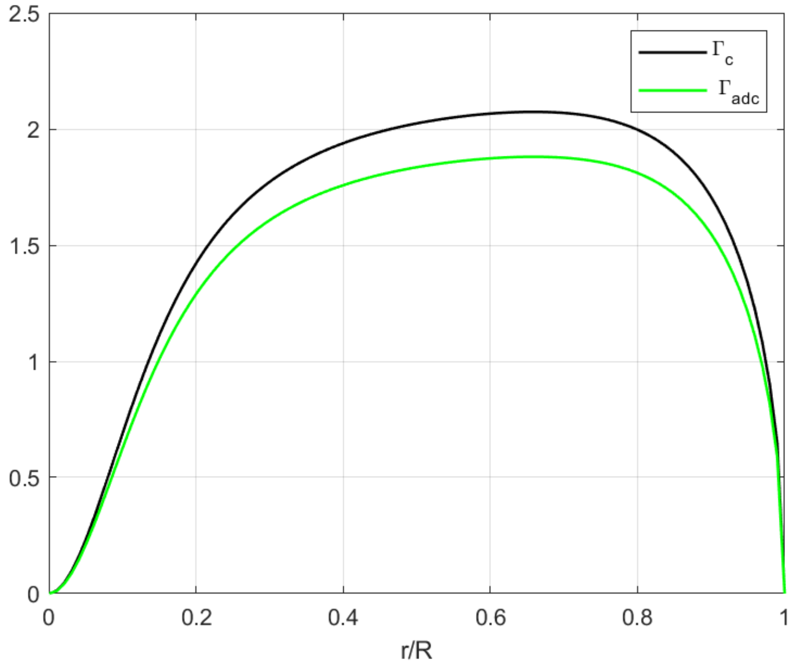

Figure 32 – Propeller 1

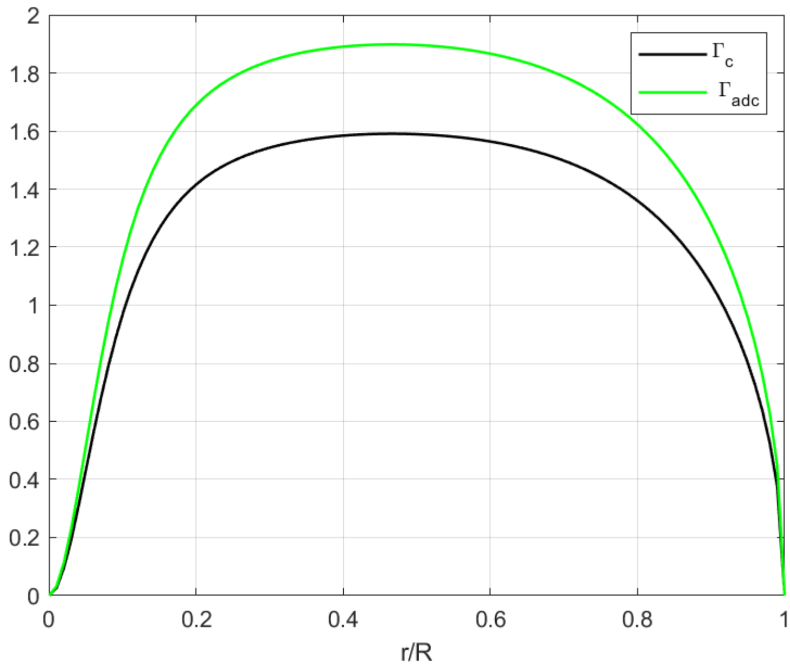

Figure 33 - Propeller 2

The relative speed (v_0) between the disk and the swirling surfaces is:

- Propeller 1: 12.02 $[m/s]$
- Propeller 2: 9.4 $[m/s]$

Finally, the axial velocity of the disk is determined, which is calculated as:

$$v_i = \frac{1}{2}\sqrt{\frac{\Gamma_{corr}(r)\Omega}{\pi}} \tag{6.8}$$

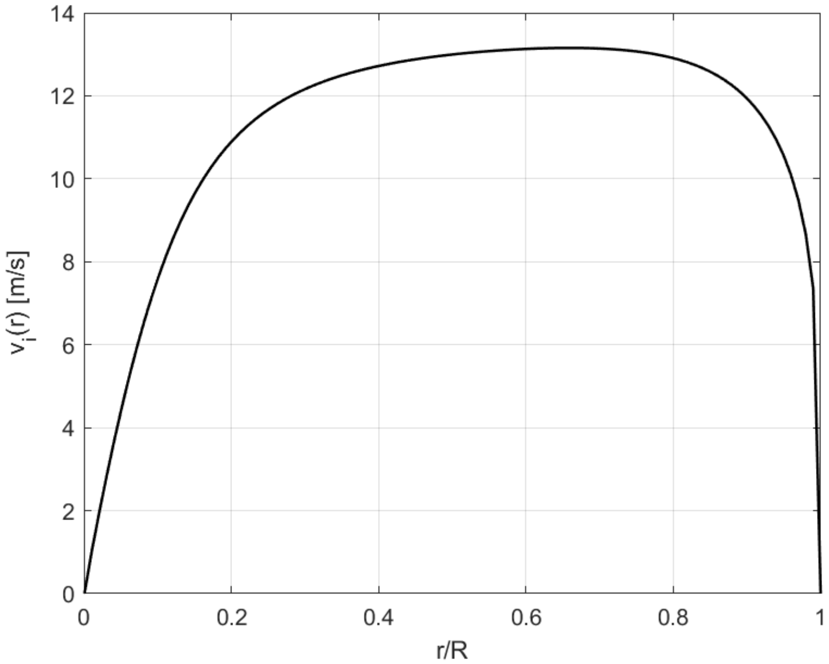

Figure 34 - Propeller 1 axial velocity

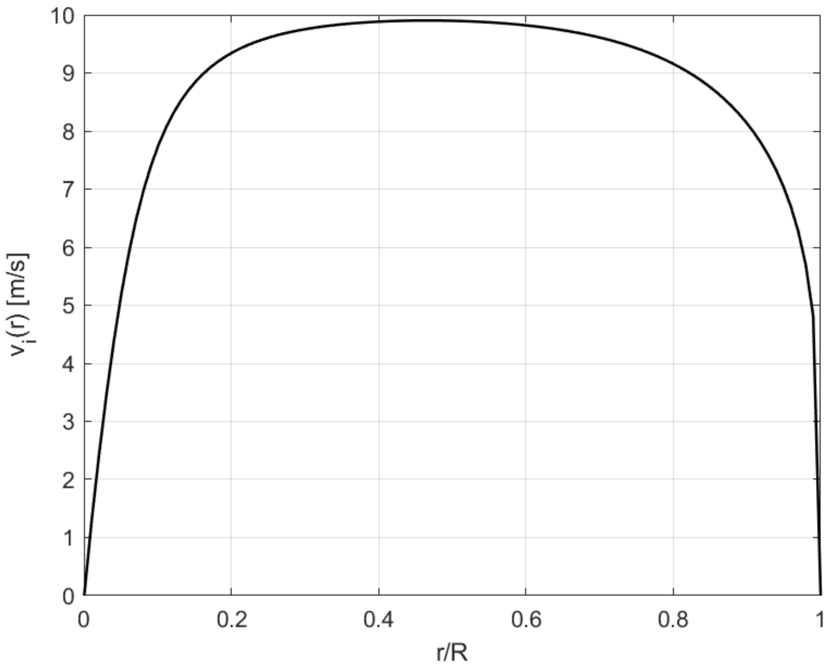

Figure 35 - Propeller 2 axial velocity

The propeller 1 has a higher distribution of values because the equation (6.8) is proportional to the square circulation and angular velocity, which in the propeller 1 are higher than propeller 2.

6.3 – Propellers Geometry

The Blade Element Theory is applied to determine the geometry of the rotors, shown in chapter 3, which allows the identification of the distribution of the chords and the distribution of pitch angle. The aerodynamic characteristics, such as the lift coefficient and the drag coefficient, are determined by an analysis of profiles conducted on XFOIL.

The pitch angle is determined by equation (3.3), as explained in paragraph 6.2.2, it is necessary to pay attention to the inflow angle to be used.

The distribution of the chords is identified as:

$$c(r) = \frac{2\, dT/dr}{\rho \cdot \cos(\phi)(\Omega r)^2 C_l} \tag{6.9}$$

$$\frac{dT}{dr} = \frac{1}{2}\rho \cos\phi\, (\Omega r)^2 C_l c dr \tag{6.10}$$

6.3.1 – Airfoils used

To identify the type of profiles to be used for a propeller, in the case of a low Reynolds number, reference was made to: (Zalewski, 2015), (Werme, 1984).

First, the distribution and the mediated value of the Reynolds number were calculated to identify the input data to perform the analysis. Furthermore, this XFOIL study was carried out without considering the compressibility, because the average value of the Mach number along the opening is less than 0.3.

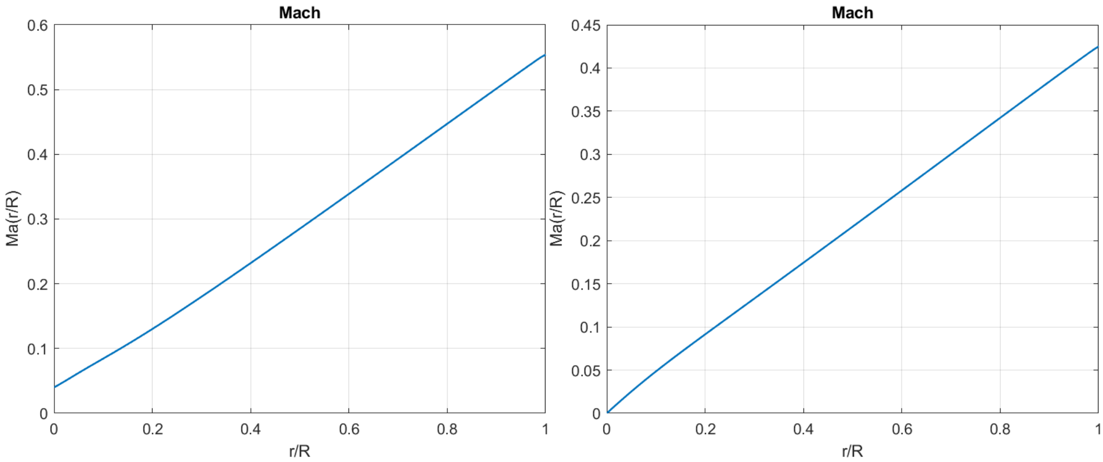

Figure 36 - Mach distribution propeller 2 and propeller 1

- Mach average propeller 2: 0.28
- Mach average propeller 1: 0.22

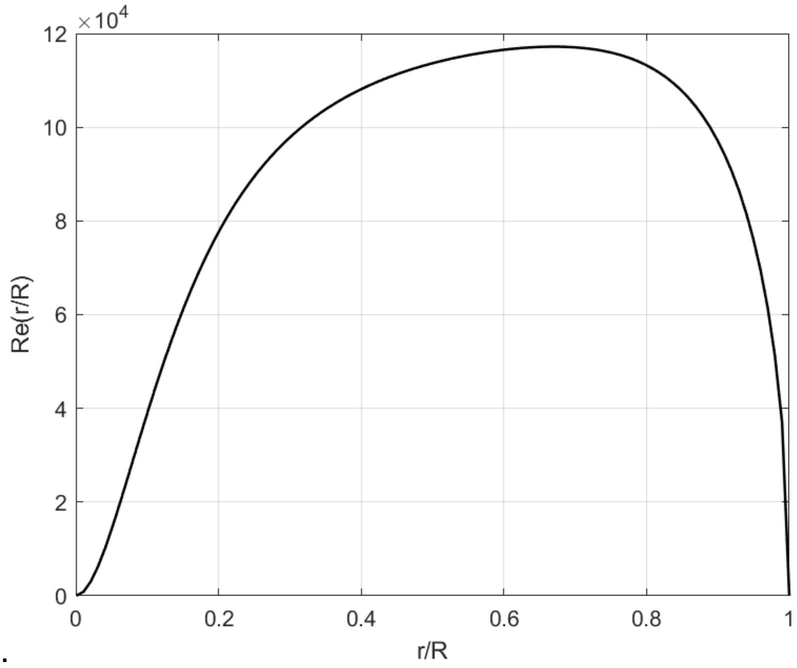

Figure 37 - Reynolds distribution propeller 1

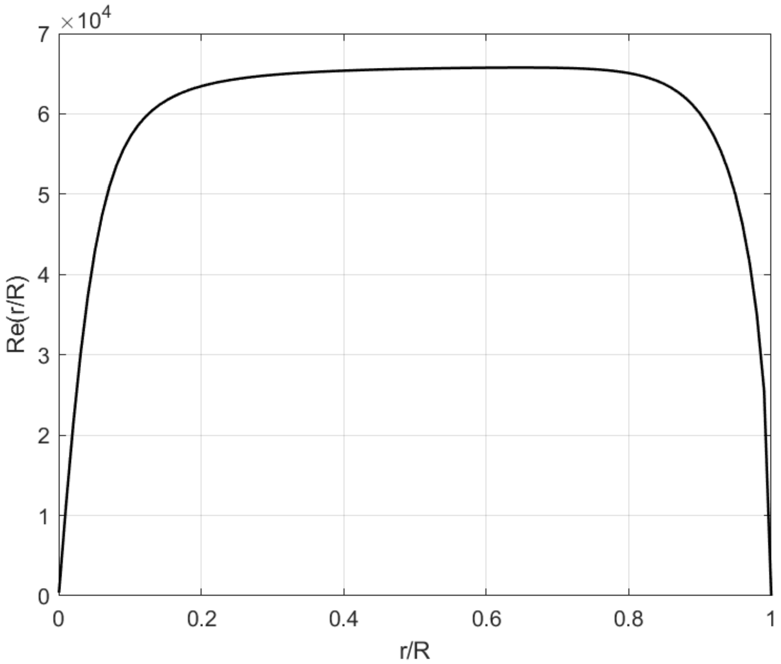

Figure 38 – Reynolds distribution propeller 2

The Reynolds number averages are:

- Propeller 1: $9 \cdot 10^4$
- Propeller 2: $6.5 \cdot 10^4$

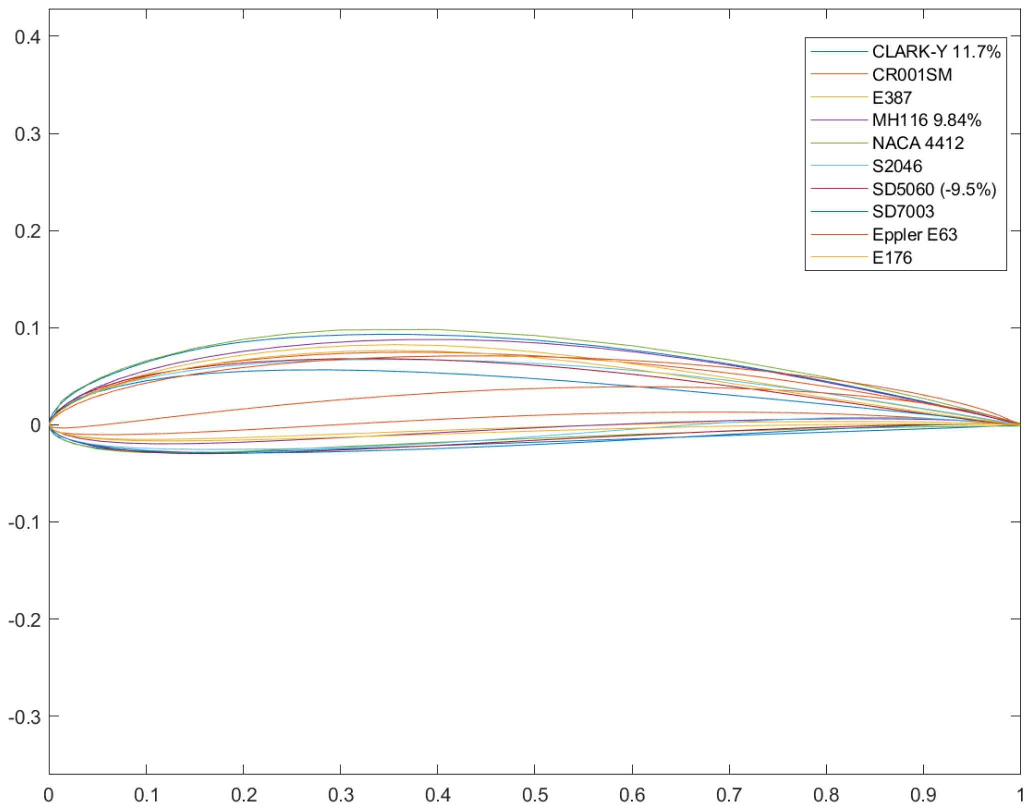

Figure 39 - Profiles analyzed

Figure 38 shows all the profiles analyzed for the indicated Reynolds numbers.

Only two profiles have been chosen (Figure 39), CLARK-Y and MH116, which have a very similar thickness and similar aerodynamic characteristics, then the distribution determined by XFOIL is reported below, and which of the two is chosen for each propeller.

- **Propeller 1**

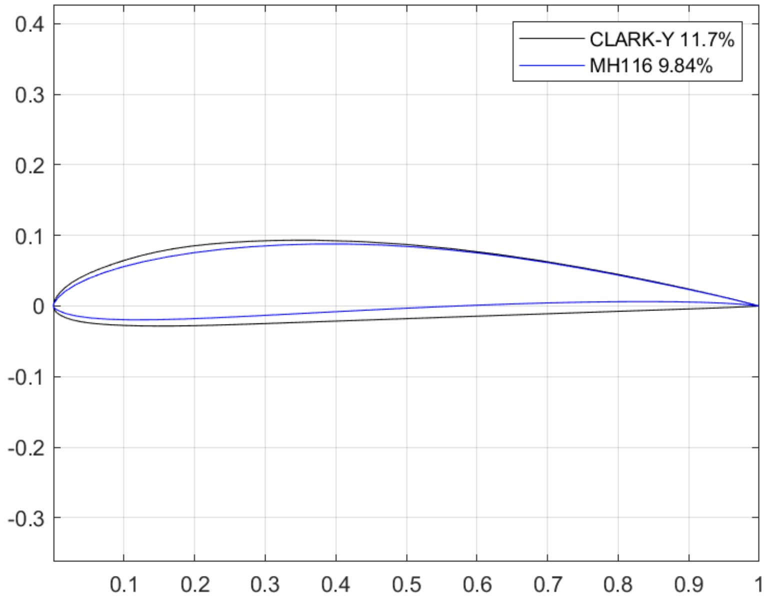

Figure 40 – Chosen profiles

  - <u>MH116 9.84%</u>

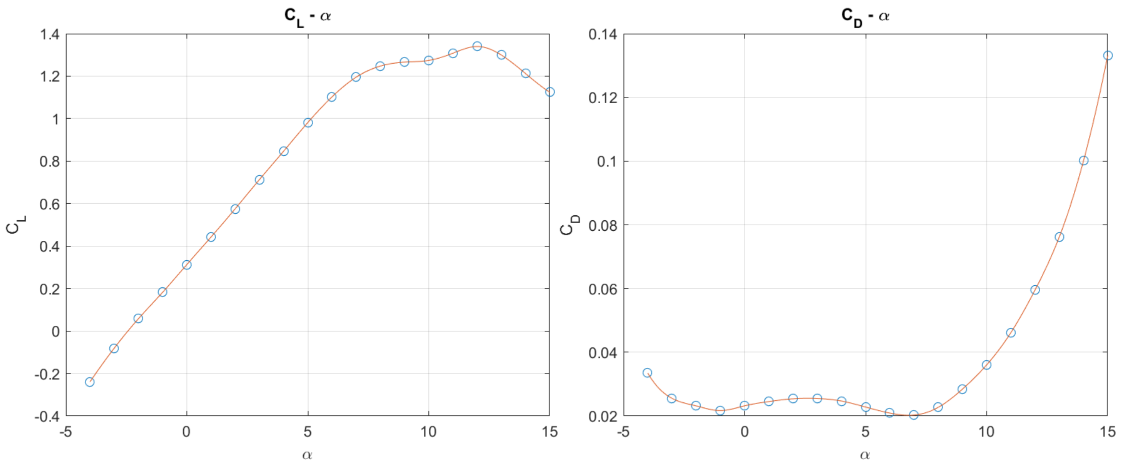

Figure 41 - Lift and drag coefficient

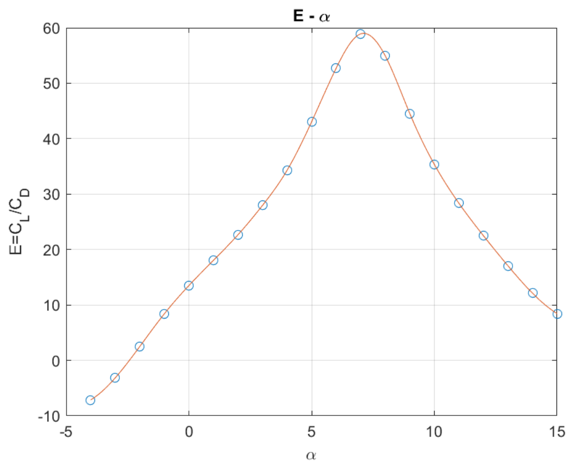

Figure 42 - Efficiency

- <u>CLARK-Y 11.7%</u>

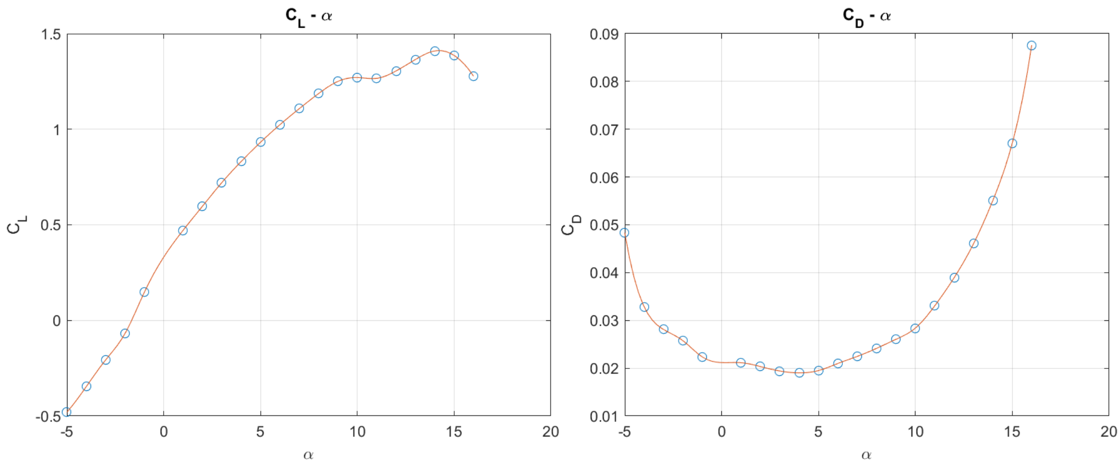

Figure 43 - Lift and drag coefficient

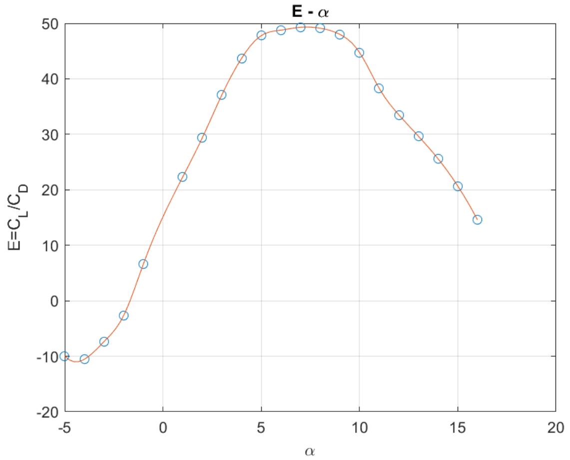

Figure 44 - Efficiency

The CLARK-Y profile has a maximum efficiency of 49 compared to the MH 116 profile which has an efficiency of 59, moreover the following profile is characterized by a slightly lower thickness than the CLARK-Y, in fact, MH 116 has a range of incidence angles with lower resistance than the CLARK-Y.

Table 6 contains all the aerodynamic characteristics calculated at the operating angle. The angle of incidence is chosen at 8° and constant throughout the blade. This angle is chosen to have maximum efficiency.

Table 6 - Aerodynamic characteristics

α_{oper}	$8°$
$C_{l_{Clark-y}}$	1.1868
$C_{l_{MH116}}$	1.2474
$C_{d_{Clark-y}}$	0.0242
$C_{d_{MH116}}$	0.0227

The chosen profile is the MH 116 thanks to the high efficiency and the wide range characterized by low resistance

In Figure 45 is report the chords distribution and in Figure 47 the pitch distribution.

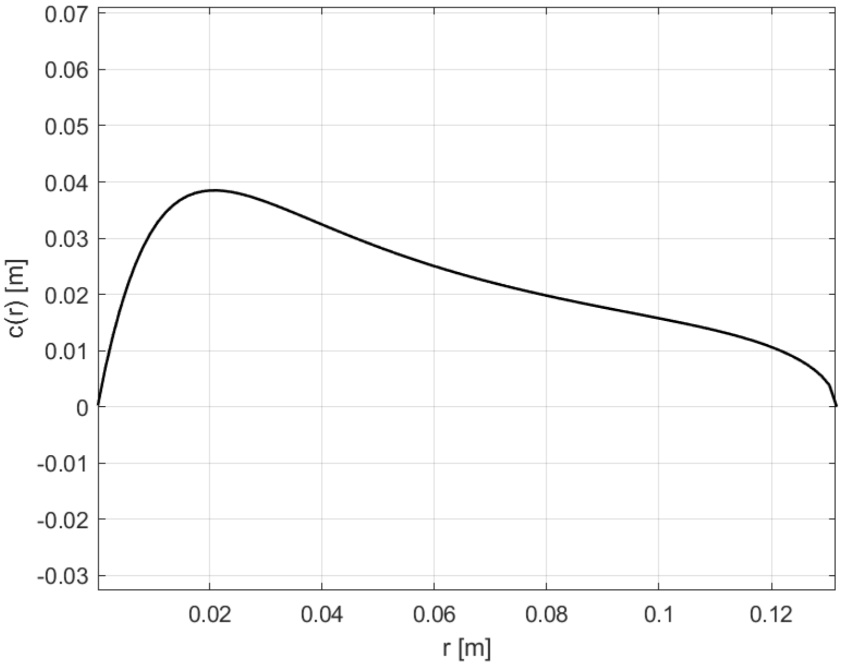

Figure 45 - Chord distribution

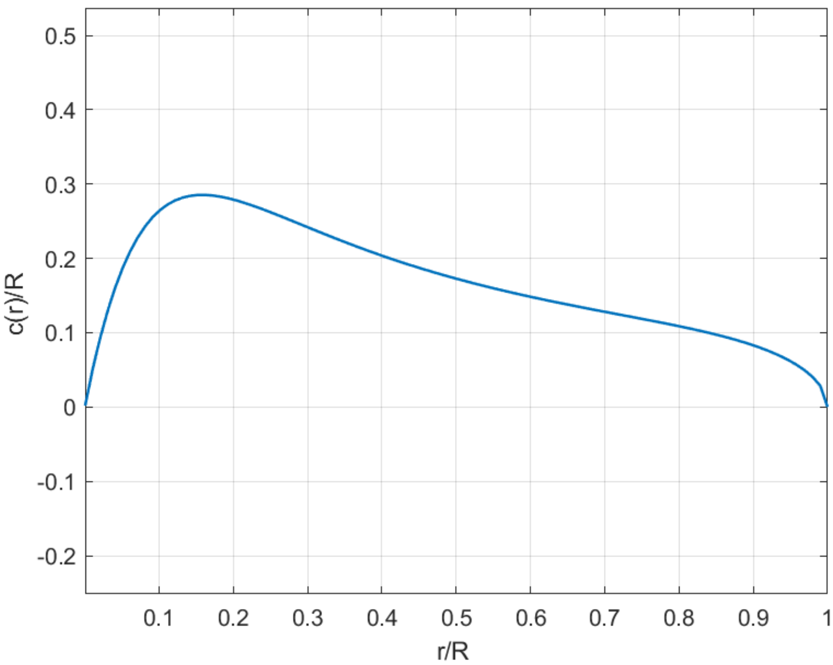

Figure 46 – Chords normalized

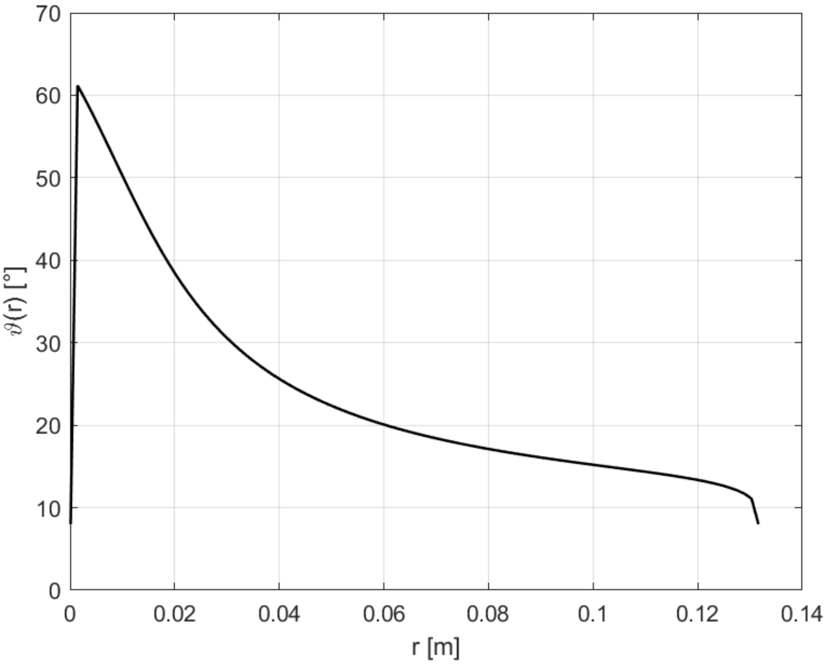

Figure 47 - θ distribution

Table 7 - Coefficients Max. propeller 1

	MH116
α_{Max}	12
C_{lMax}	1.3395
C_{dMax}	0.0595

- **Propeller 2**

Also, for this propeller, the chosen profiles are shown in Figure 40

  - <u>CLARK-Y 11.7%</u>

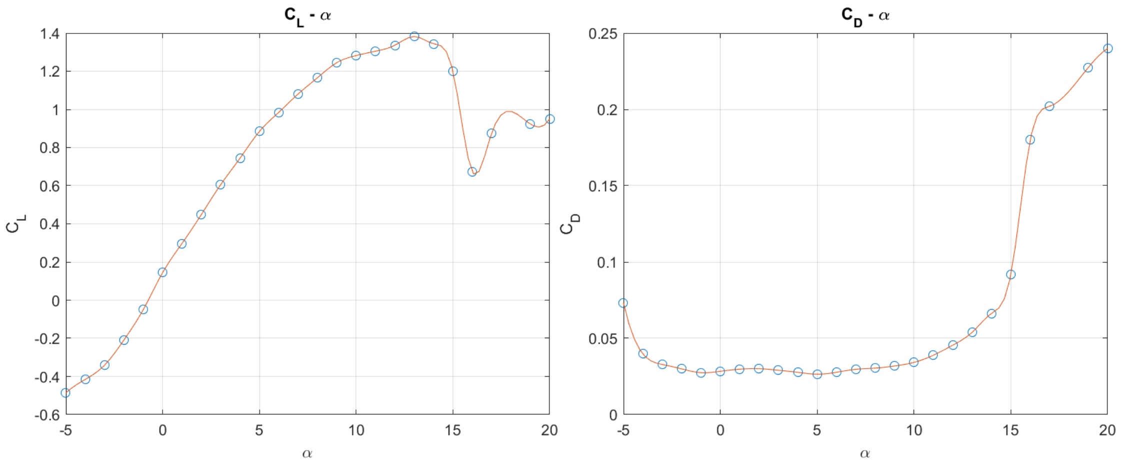

Figure 48 - Lift and drag coefficient

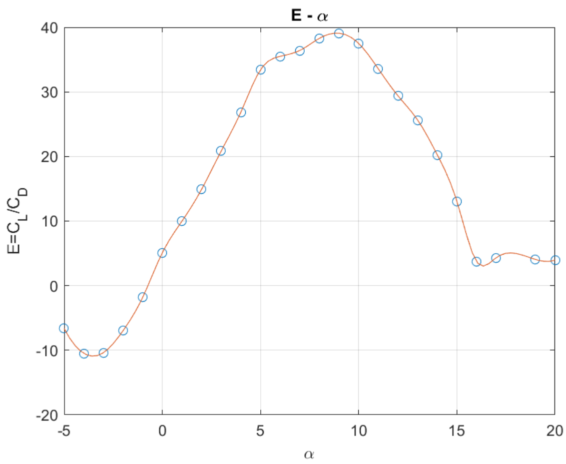

Figure 49 - Efficiency

- ○ <u>MH 116 9.84%</u>

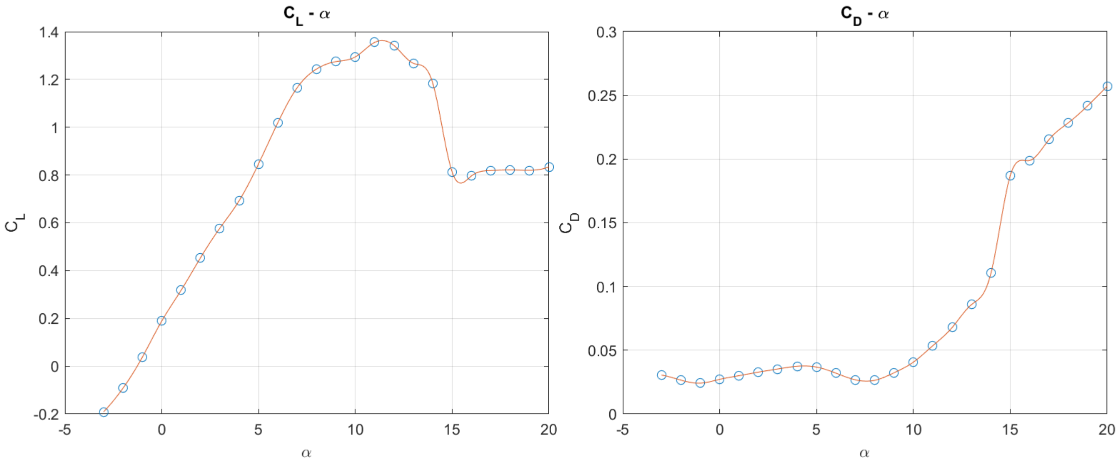

Figure 50 - Lift and drag coefficient

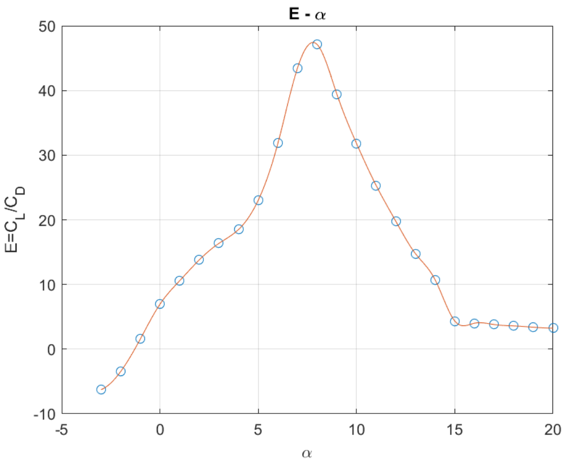

Figure 51 – Efficiency

Table 8 - Aerodynamic characteristics

α_{oper}	8°
$C_{l_{Clark-y}}$	1.16
$C_{l_{MH116}}$	1.24
$C_{d_{Clark-y}}$	0.03
$C_{d_{MH116}}$	0.026

Also in this case, the MH116 profile is chosen because it has a higher efficiency than the CLARK-Y, moreover considering the operating angle, which corresponds to the maximum efficiency angle.

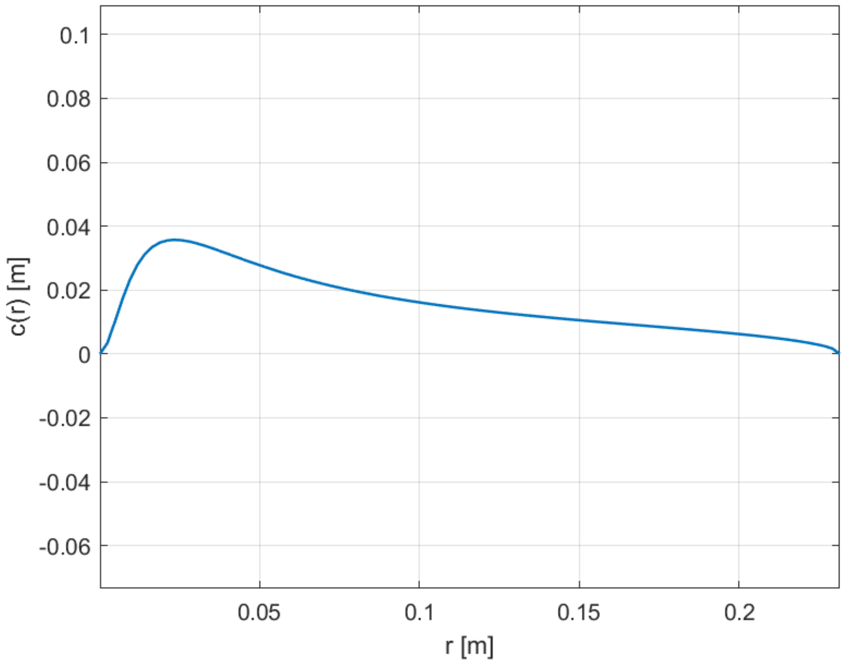

Figure 52 – Chords distribution

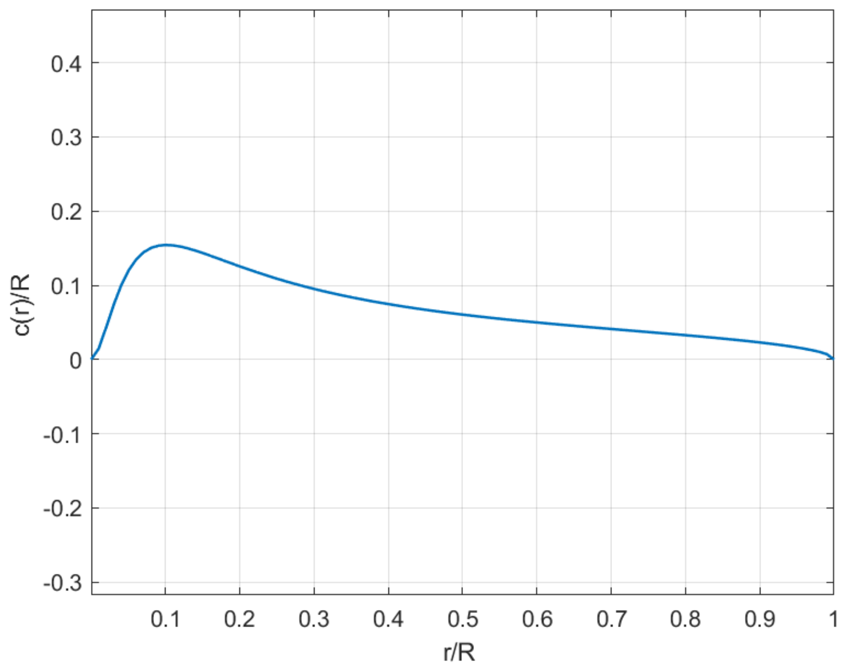

Figure 53 - Chords normalized

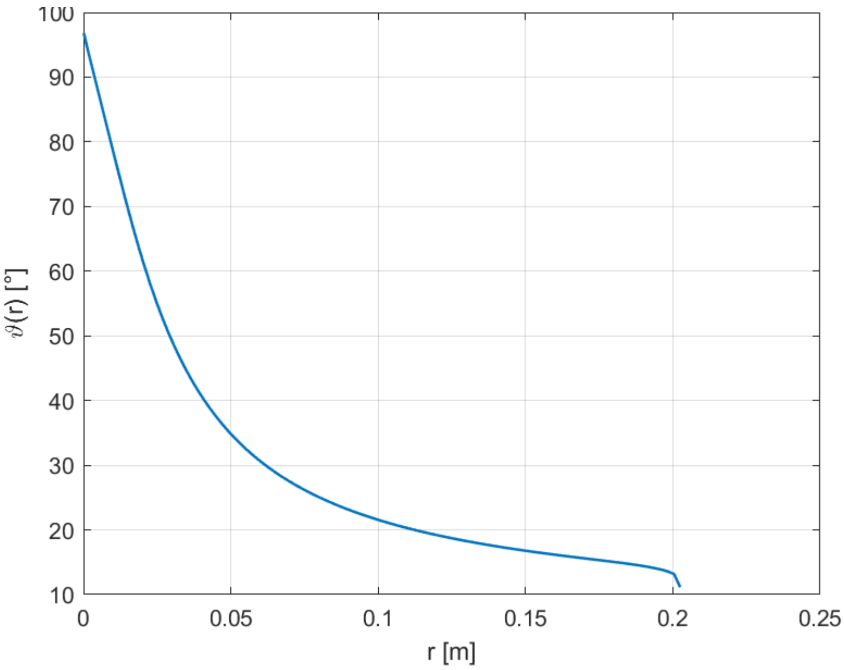

Figure 54 – θ first method

Table 9 - Coefficients Max. propeller 2

	MH116
α_{Max}	11.36
C_{lMax}	1.36
C_{dMax}	0.06

6.4 – Propeller performance

In the following paragraph, the performances of the two propellers are calculated by referring to the Blade Element Theory in chapter 3, in particular reporting the results of the equations: (3.25), (3.26), (3.27), (3.23).

Table 10 - Propeller 1 performance

Propeller 1	
C_P	0.038726
C_Q	0.006163
C_T	0.117536
$F.M.$	0.8465
$F.M.25\%$	0.7521
$T[N]$	13.74
$Q[N \cdot m]$	0.19
$P[W]$	196.34
$T_{25\%}\ [N]$	13.285

Table 11 - Propeller 2 performance

Propeller 2	
C_P	0.019961
C_Q	0.003177
C_T	0.038081
J	0.072461
$F.M.$	0.3180
$F.M.25\%$	0.285
$T\ [N]$	23.29
$Q\ [N \cdot m]$	0.89
$P[W]$	688.14
$T_{25\%}\ [N]$	22.13

Table 11 also calculates the advance ratio, because for propeller 2 is considered the cruise speed.

6.5 – Induced field

The equations given in chapter 5 are used to determine the induced flow field, in particular (5.44), (5.42).

The domain is evaluated from $z = -5[m]$ to $z = 5\ [m]$. The radius goes from 0 to R, which in the case of the propeller 1 is 0.1316 [m], while for the propeller 2, the value is: 0.2316 [m]. Thanks to these intervals, it is possible to determine a grid to analyze the flow.

The tangential speed does not depend on the distance from z, for this reason, the distribution evaluated in chapter 4 is shown in Figure 55 and 56 for both propellers.

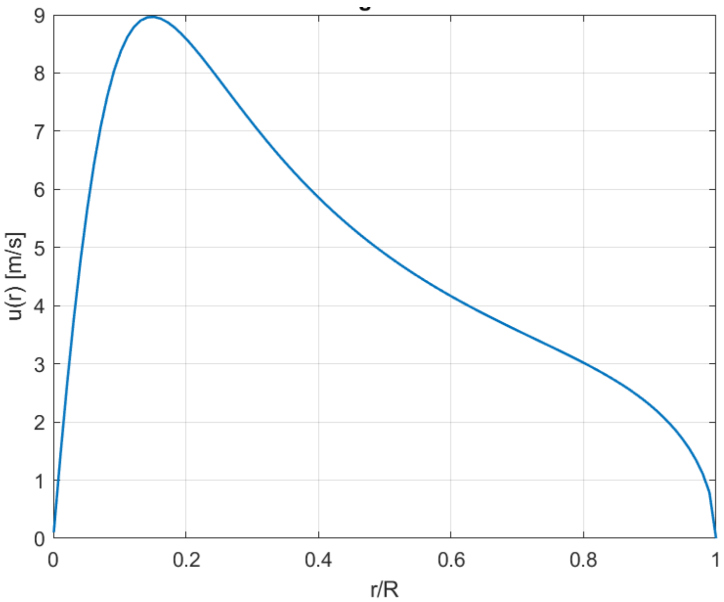

Figure 55 – tangential speed, propeller 1

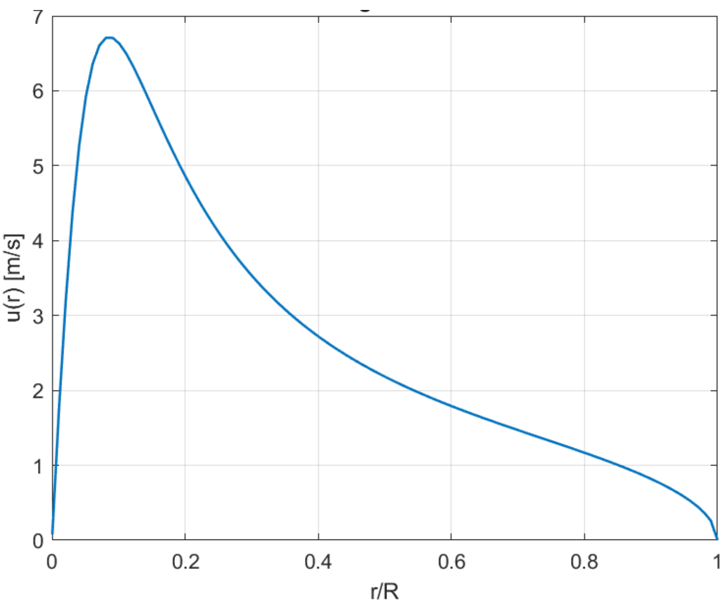

Figure 56 - Tangential speed, propeller 2

The axial velocities are reported based on the proximity to the disk, both for the propeller 1 and the propeller 2.

- Propeller 1

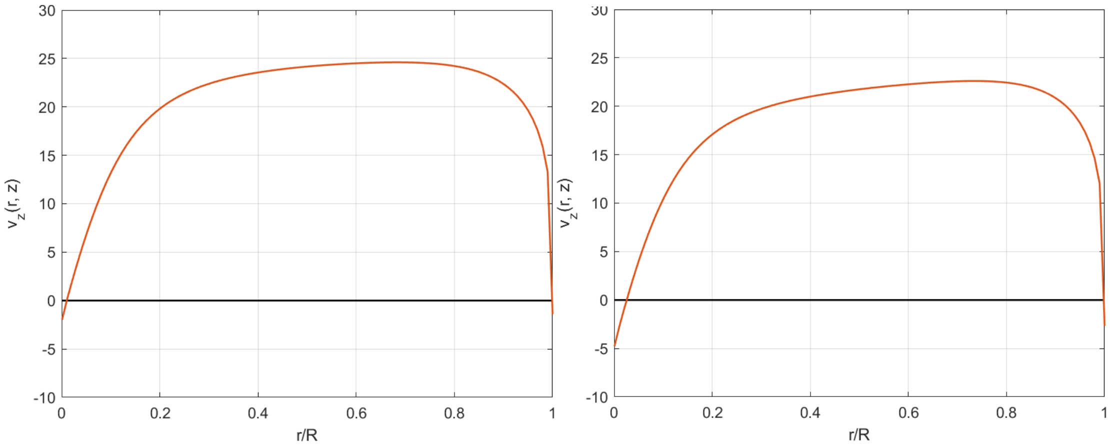

Figure 57 – Axial velocity for z=0.64R and z=0.32R

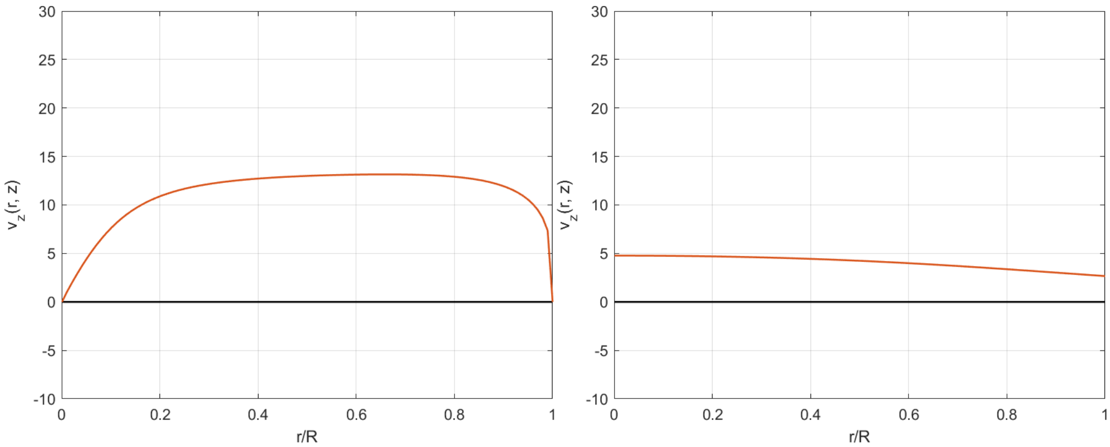

Figure 58 - Axial velocity for z=0 and z=-0.32R

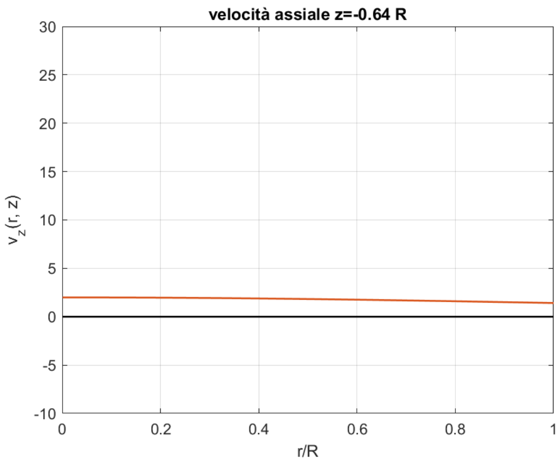

Figure 59 - Axial velocity for z=-0.64R

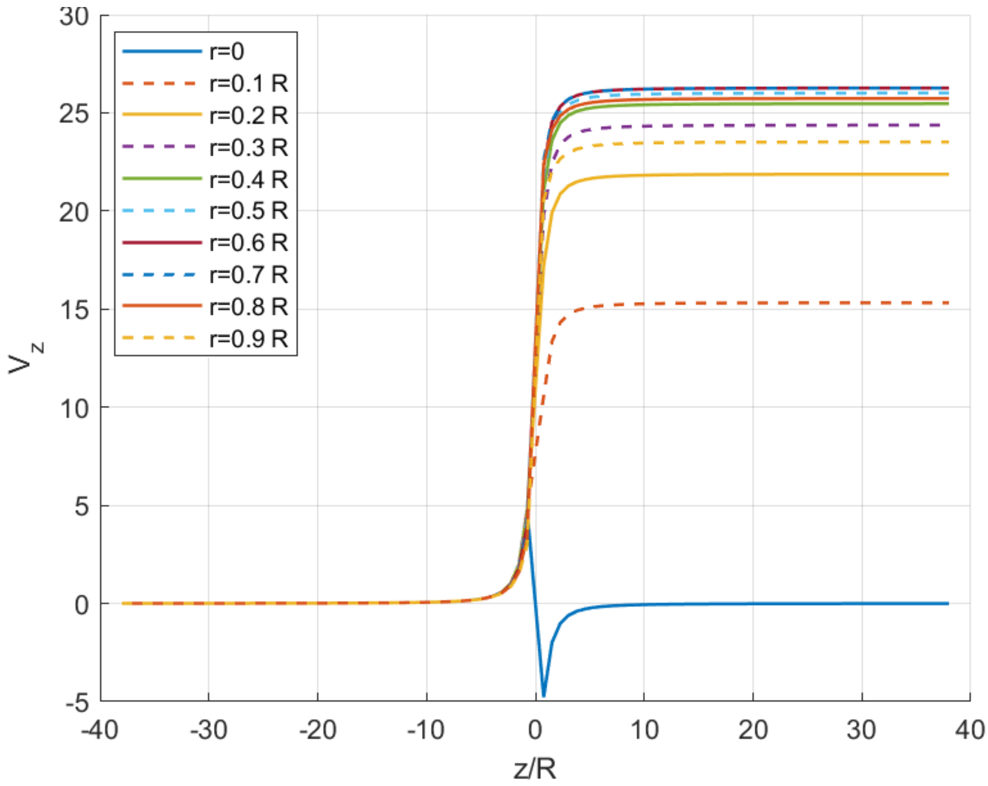

Figure 60 - Axial Velocities

- Propeller 2

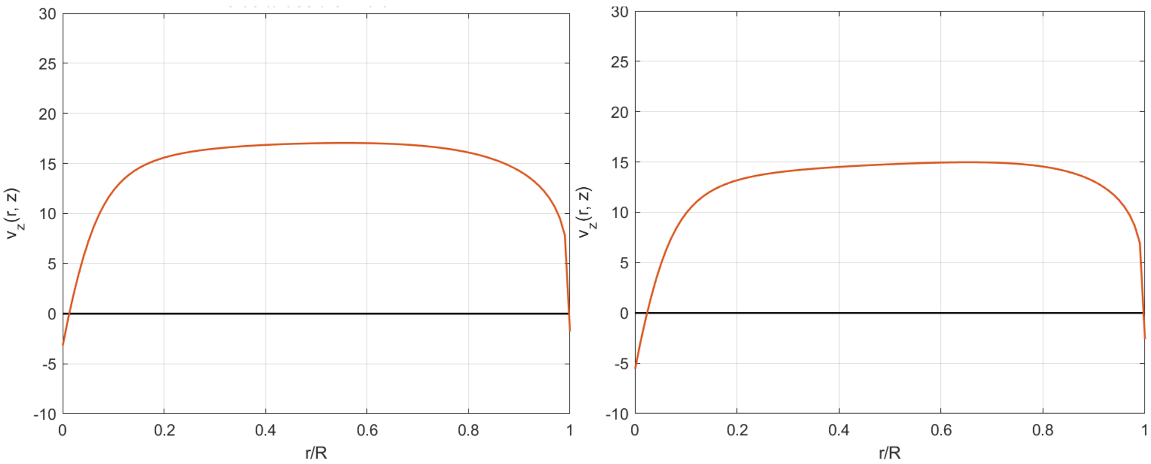

Figure 61 - Axial velocity for z=0.64R and z=0.32R

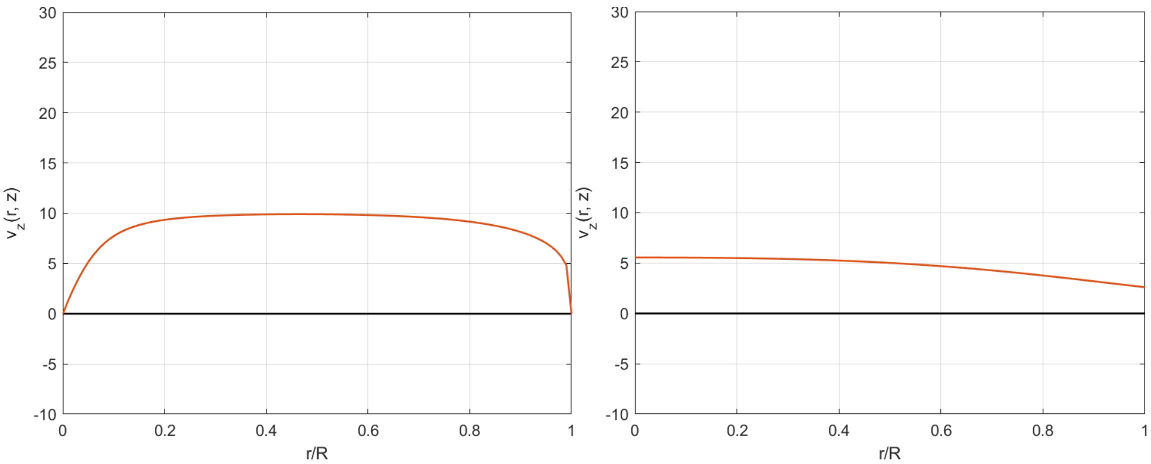

Figure 62 - Axial velocity for z=0 and z=-0.32R

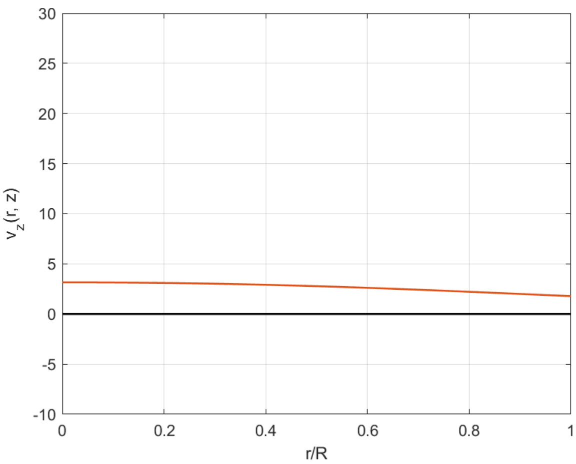

Figure 63 - Axial velocity for z=-0.64R

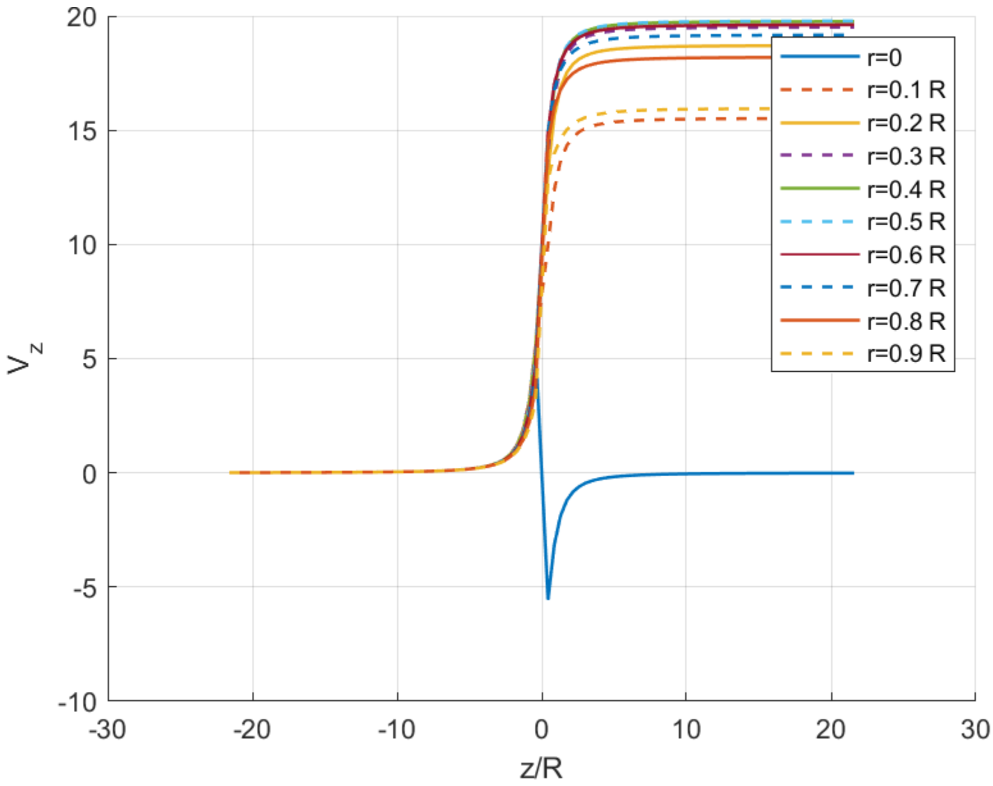

Figure 64 - Axial Velocities

6.6 – CAD

Propeller 1

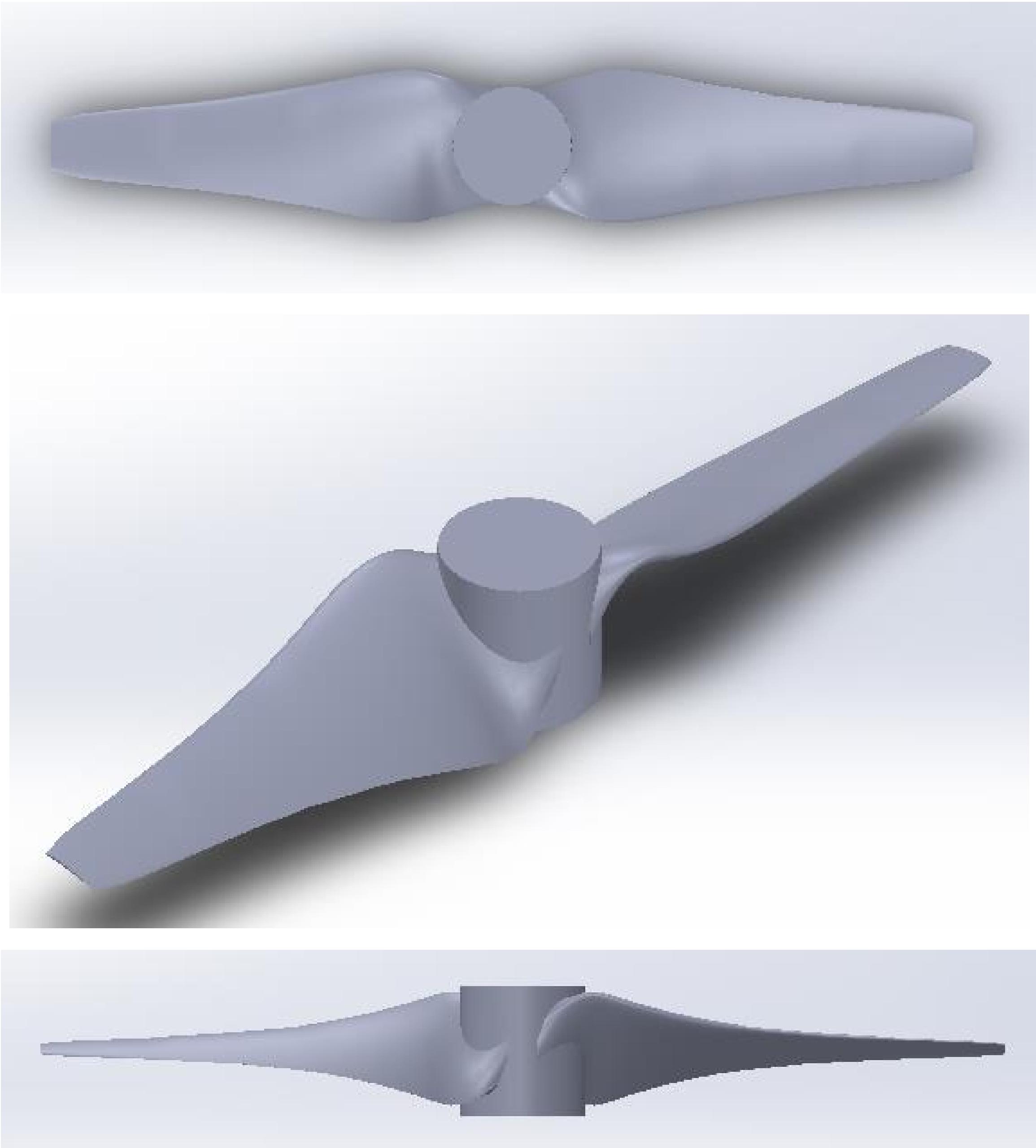

Figure 65 - Propeller 1 CAD

Propeller 2

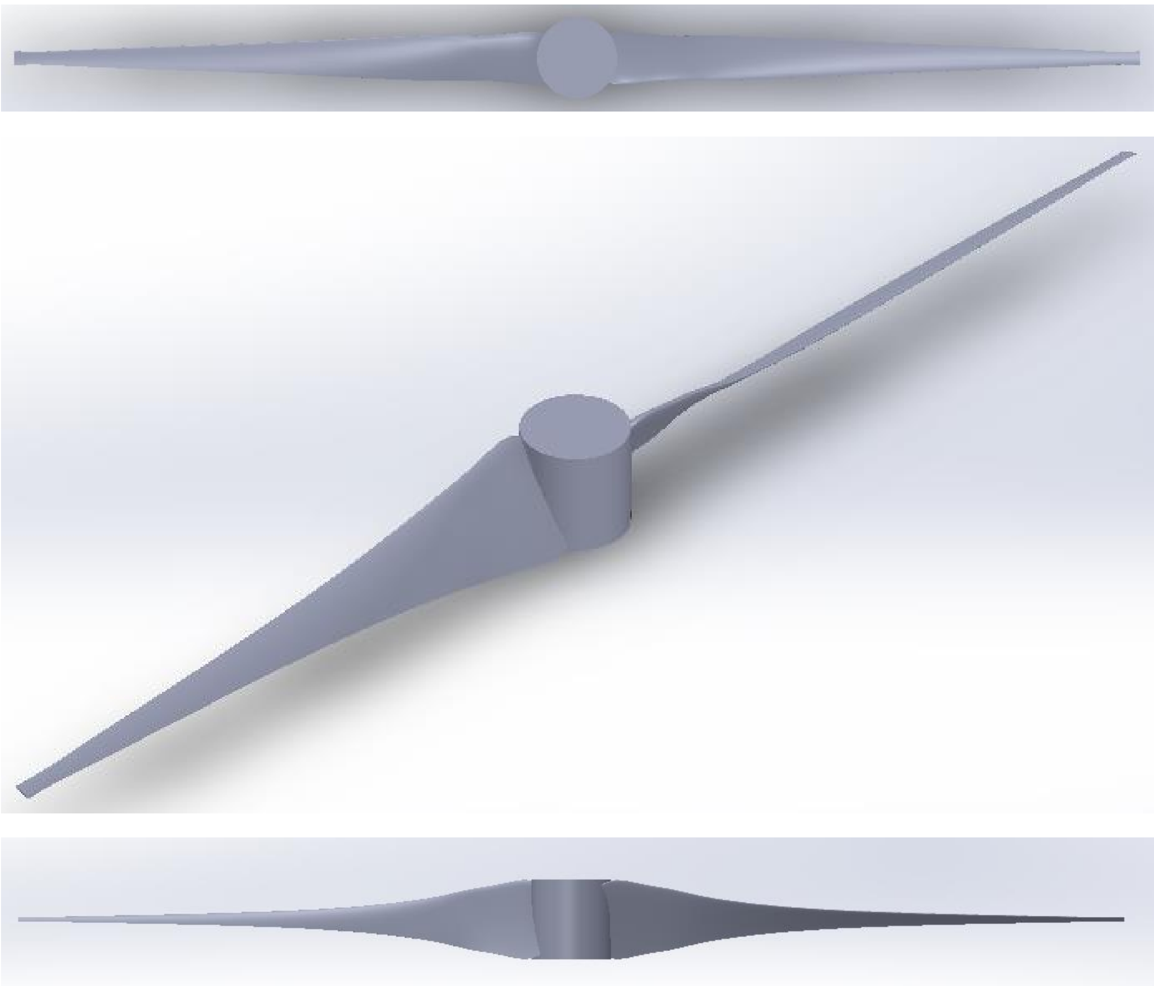

Figure 66 - Propeller 2 CAD

Table 12 - Geometry of the propeller 1

Stations	Chords	Pitch
1	0,037	38,71
2	0,0352	33,78
3	0,0331	30,01
4	0,0308	27,09
5	0,0286	24,81
6	0,0266	22,99
7	0,0248	21,52
8	0,0231	20,29
9	0,0216	19,26
10	0,0203	18,39
11	0,0190	17,63
12	0,0179	16,97
13	0,0168	16,39
14	0,0157	15,86
15	0,0146	15,36
16	0,0134	14,89
17	0,0120	14,42
18	0,0102	13,91
19	0,0075	13,30
20	0	12,44

Table 13 - Geometry of the propeller 2

Stations	Chords	Pitch
1	0,0354	77,98
2	0,0322	64,96
3	0,0283	54,61
4	0,0248	46,88
5	0,0219	41,11
6	0,0195	36,71
7	0,0175	33,28
8	0,0158	30,54
9	0,0143	28,32
10	0,0131	26,47
11	0,0120	24,92
12	0,0110	23,59
13	0,0100	22,43
14	0,0091	21,42
15	0,0082	20,51
16	0,0073	19,68
17	0,0063	18,92
18	0,0051	18,18
19	0,0036	17,45
20	0	16,62

The station 20 has not been reported for both propellers, while station 1 refers to 15% of the total radius for the propeller 1 and to 7% of the total radius of the propeller 2 to obtain a hub of about 3.2 cm for both propellers. Furthermore, the choice of hub dimensions is related to that used for the first propeller of the Skywalker X8, which is the one used for low altitude operations.

Conclusions

In the following study, several models have been implemented with them is possible to represent the composition of motion. Initially, the two impulsive theories were implemented; with the Simple Impulsive Theory the induced power was determined without taking into account the rotation of the wake, while with the extended impulsive theory the rotation of the wake is considered, in fact, the flux in addition to having a given axial speed also has a tangential speed. The two theories have been implemented for 600 scenarios, in particular, 20 masses and 30 diameters.

However, more sophisticated theories have been implemented, such as the Vortex Theory, which has been adapted to the Blade Element Theory. With the vortex theory, it is possible to obtain the circuitry in optimal condition through the Glauert parameter (G) and the velocity field components.

Subsequently, having chosen a profile with high aerodynamic performances on the base of the Reynolds number obtained, the geometries of the two propellers were determined by the Blade Element Theory.

By applying the linearized theory of the actuator disk, the axial velocity was obtained for a flow tube of a given size.

It is necessary to validate the study done with:

- Perform CFD analysis on the propellers for vertical take-off
- Perform CFD analysis on the driving propeller
- Check how the front propellers act on the rear
- Check out the motion field produced by the propellers for vertical take-off on the driving propeller
- Check how the body of the drone changes the range of motion of the propellers
- Of course, the analyzes must be conducted considering a real flow and compressibility, which reduces the aerodynamic characteristics.

Bibliography

1. A. R. S. Bramwell, G. D. (2001). *Bramwell's Helicopter Dynamics.* Butterworth-Heinemann.
2. Besset, A. B. (1888). *Hydrodynamics with numerous examples Vol. 2.* London: George Bell and Sons.
3. Conway, J. T. (1997). *Exact actuator disk solutions for non-uniform heavy loading and slipstream contraction.* Grimstad: Cambridge University Press.
4. J. D. Anderson, J. (2011). *Fundamentals of Aerodynamics.* Mc Graw Hill.
5. J. Seddom, S. N. (2011). *Basic Helicopter Aerodynamics.* Wiley.
6. Johnson, W. (1994). *Helicopter Theory.* New York: Dover Publications, INC.
7. Johnson, W. (2013). *Rotorcraft Aeromechanics.* New York: Cambridge University press.
8. M. Knighr, R. A. (1937). *Static thrust analysis of the lifting airscrew.* Washington: National Thechnical Information Service.
9. Peters, R. M.-D. (2016). *Optimum blade loading for a power rotor in descent.* St. Louis: Chinese Journal of Aeronautics.
10. Saha, K. (2008). *The Earth's Atmosphere its physics and dynamics.* Berlin: Springer.
11. Sørensen, J. N. (2016). *General Momenthum Theory for Horizontal Axis Wind Turbines Vol. 4.* Lyngby: Springer.
12. Werme, J. F.-T. (1984). *Clark-Y Airfoil Performance at Low Reynolds Numbers.* Reno: AIAA 22nd Aerospace Sciences Meeting.
13. Zalewski, W. (2015). *A study of propeller for high altitude unmanned airplane.* Warsaw: Journal of KONES Powertrain and Transport.
14. Zazza, D. (2017). *Analisi delle prestazioni e del campo di moto indotto da un elica in ambiente marziano.*

Sitography

https://www.apcprop.com/technical-information/performance-data/

https://m-selig.ae.illinois.edu/props/propDB.html